COMPRESSION AND SHEAR WAVE PROPAGATION IN EXPLOSIVES

January 1989

Final Report

By: M. Cowperthwaite
Contributor: Y. M. Gupta

Prepared for:

U. S. ARMY RESEARCH OFFICE
P. O. BOX 12211
Research Triangle Park, NC 22709-2211

Contract No. DAA29-84-K-0018

SRI Project PYU-6834

SRI International
333 Ravenswood Avenue
Menlo Park, California 94025-3493
(415) 326-6200
TWX: 910-373-2046
Telex: 334486

REPORT DOCUMENTATION PAGE

1a. REPORT SECURITY CLASSIFICATION UNCLASSIFIED	1b. RESTRICTIVE MARKINGS N/A since Unclassified
2a. SECURITY CLASSIFICATION AUTHORITY N/A since Unclassified	3. DISTRIBUTION/AVAILABILITY OF REPORT Approved for public release; distribution unlimited.
2b. DECLASSIFICATION/DOWNGRADING SCHEDULE N/A since Unclassified	
4. PERFORMING ORGANIZATION REPORT NUMBER(S) SRI Project PYU-6834	5. MONITORING ORGANIZATION REPORT NUMBER(S) ARO 21117.2-EG
6a. NAME OF PERFORMING ORGANIZATION SRI International 6b. OFFICE SYMBOL (If applicable)	7a. NAME OF MONITORING ORGANIZATION U.S. Army Research Office
6c. ADDRESS (City, State, and ZIP Code) 333 Ravenswood Avenue Menlo Park, CA 94025-3493	7b. ADDRESS (City, State, and ZIP Code) P.O. Box 12211 Research Triangle Park, NC 27709-2211
8a. NAME OF FUNDING/SPONSORING ORGANIZATION 8b. OFFICE SYMBOL (If applicable)	9. PROCUREMENT INSTRUMENT IDENTIFICATION NUMBER DAA29-84-K-0018
8c. ADDRESS (City, State, and ZIP Code)	10. SOURCE OF FUNDING NUMBERS PROGRAM ELEMENT NO. / PROJECT NO / TASK NO / WORK UNIT ACCESSION NO

11. TITLE (Include Security Classification)
COMPRESSION AND SHEAR WAVE PROPAGATION IN EXPLOSIVES

12. PERSONAL AUTHOR(S)
Cowperthwaite, M.

13a. TYPE OF REPORT	13b. TIME COVERED	14. DATE OF REPORT (Year, Month, Day)	15. PAGE COUNT
Final	FROM 840201 TO 880930	890100	84

16. SUPPLEMENTARY NOTATION The view, opinions and/or findings contained in this report are those of the author(s) and should not be construed as an official Department of the Army position, policy, or decision, unless so designated by other documentation.

17. COSATI CODES		
FIELD	GROUP	SUB-GROUP
19	09	
20	11	

18. SUBJECT TERMS (Continue on reverse if necessary and identify by block number)
Normal impact
Parallel-inclined impact (PII)
Lagrange particle velocity gages
Explosives
Composition B3

19. ABSTRACT (Continue on reverse if necessary and identify by block number)

This report presents our experimental and theoretical studies of compression and shear wave propagation in explosives. The objective of the experimental study was to establish and investigate the occurrence of shear-induced reaction (SIR) in an explosive subjected to the type of one-dimensional compression and shear (1DCS) loading produced by the parallel-inclined impact (PII) technique pioneered by Gupta. The objective of the theoretical study was to formulate a treatment of the reactive flow produced in an explosive subjected to 1DCS loading and thereby provide a framework for interpreting the results of the PII experiments.

Our theoretical study was based on a model analysis of the PII experiment with the shock-loaded target treated as an inert elastic solid and the resulting flow treated ideally as a pure compression wave followed by a pure shear wave. A complete equation

20. DISTRIBUTION/AVAILABILITY OF ABSTRACT ☒ UNCLASSIFIED/UNLIMITED ☐ SAME AS RPT. ☐ DTIC USERS	21. ABSTRACT SECURITY CLASSIFICATION Unclassified
22a. NAME OF RESPONSIBLE INDIVIDUAL	22b. TELEPHONE (Include Area Code) / 22c. OFFICE SYMBOL

18. SUBJECT TERMS (Continued)

Longitudinal particle velocity histories
Compression waves
Shear waves
Reactive elastic solids
Shear-induced reaction (SIR)
Compression-induced reaction (CIR)
Shock-induced reactive flow

19. ABSTRACT (Continued)

of state (EOS) for a reactive elastic solid was formulated and used to derive the thermodynamic equations governing the one-dimensional adiabatic flows produced by PII. The conditions an elastic solid must satisfy to produce our ideal inert flow when subjected to PII were then formulated and used to construct the most convenient model EOS for investigating the reactive adiabatic flows produced in solids by normal-impact and PII. Flows influenced by compression-induced reaction (CIR) and SIR were then considered to show how the energy released by chemical reaction influences the longitudinal particle velocity field.

Our experimental study was based on Gupta's premise that significant differences between the sets of longitudinal particle velocity histories recorded in an explosive subjected to normal impact and PII producing equivalent nonreactive compression waves can be taken as evidence for the occurrence of SIR in the PII experiment. Eighteen normal-impact and PII experiments were performed in a gas gun with Composition B3 targets, and multiple Lagrange gages embedded in these explosive targets were used to make longitudinal and shear particle velocity measurements. The eighteen experiments were divided into five sets that were performed with targets made from different batches of Composition B3. The results of the longitudinal particle velocity measurements gave evidence for the occurrence of SIR in the first batch of Composition B3, which was shocked initially into the 10-kbar region, and in the fifth batch of Composition B3, which was shocked initially into the 15-kbar region. The results of the shear particle measurements led to the conclusion that the shear deformation produced in Composition B3 by PII remains close to the impact surface.

PREFACE

We gratefully acknowledge many contributions that were made to this work by our colleagues and coworkers. We are especially indebted to Dr. Y. M. Gupta of Washington State University for his interest in this work and his assistance in designing the gas gun experiments. We sincerely thank the following persons at SRI for their contributions to this work. The gas gun assemblies were expertly fabricated by D. Henley, who also contributed to many experimental designs and ideas. The Composition B3 charges were cast by H. E. Hanna. The gas gun experiments were performed by D. Walter, with technical assistance from F. Galimba and C. Flohr. The data reduction was performed by B. Bain and B. Y. Lew.

CONTENTS

TABLE OF CONTENTS (Continued)

LIST OF ILLUSTRATIONS

LIST OF ILLUSTRATIONS (Continued)

1. INTRODUCTION

This report presents our experimental and theoretical studies of compression and shear wave propagation in explosives. The objective of the experimental study was to establish and investigate the occurrence of shear-induced reaction (SIR) in an explosive subjected to one-dimensional compression and shear (1DCS) loading. The objective of the theoretical study was to formulate a theoretical treatment for the propagation of compression and shear waves in an explosive.

SIR in explosives was postulated in the 1940s by Bridgman,[1] and the results of explosive sensitivity tests, such as the drop-weight[2] and fragment impact tests, provide some evidence for its occurrence. Such tests cannot, however, be used to establish the occurrence of SIR, because they are not well instrumented and the explosives are subjected to different combinations of deformations that are not amenable to quantitative analysis. These limitations prompted Gupta[3] to propose the use of his 1DCS wave technique[4,5] to study SIR in explosives. In Gupta's 1DCS wave technique, the gas gun is used to perform parallel-inclined impact (PII) experiments with multiple Lagrange particle velocity gages embedded in the target. In a particular experiment, the magnetic field is oriented to allow the gages to measure either longitudinal particle velocity (u_1) histories or shear particle velocity (u_2) histories. The shear loading can be varied by changing the impact angle. These PII experiments remove the limitations inherent in the sensitivity tests because they provide us with the capability of (1) determining the dynamic shear properties of shock-loaded material,[6] (2) establishing the occurrence of SIR and its role in the initiation of an explosive, and (3) understanding the influence of SIR on the flow produced in an explosive by oblique impact.

Our experimental approach to SIR can now be introduced as an application of Gupta's 1DCS wave technique to explosives. In this

approach, longitudinal particle velocity histories are measured in normal and PII experiments designed to produce compression waves of the same strength that are nonreactive in the time frames of the experiments. In this case, because the loading conditions differ only by a shear component, significant differences between the sets of particle velocity histories recorded in the normal and PII experiments can be taken as evidence for the onset and occurrence of SIR in the explosive subjected to PII.

The explosive Composition B3 was chosen as the test explosive for our experimental investigation of SIR because it is readily available and because pucks for the gas gun experiments can readily be fabricated by casting it around a gage assembly.

Our theoretical approach to the propagation of compression and shear waves in an explosive is based on an analysis of the PII experiment with the shock-loaded target treated as an elastic solid. Because Lagrange gages are used in our PII experiment, we first introduced the Lagrange strain and the first and second Piola-Kirchhoff (PK) stresses as the natural variables for describing states attained in the reference configuration. To provide a basis for our investigation, we then introduced the ideal flow produced in an elastic solid by PII, namely, a pure, inert compression wave (CW) followed by a pure, inert shear wave (SW). A complete equation of state (EOS) for a reactive, elastic solid was then formulated and used to derive the thermodynamic equations governing the adiabatic flow produced in such a solid by PII. Conditions for an elastic solid to support the ideal flow considered earlier were then derived and incorporated into a particular EOS for a reactive solid so that we could develop the most fundamental treatment of reactive CWs and SWs produced by PII. Flows with compression-induced reaction (CIR) initiated by the CW, as well as flows with SIR initiated by the SW, were then considered to show how the chemical energy influences the longitudinal particle velocity and thereby provide a means of interpreting the results of the gas gun experiments.

Section 2 of this report describes our experimental techniques used to measure compression and shear response in gas gun experiments and also

presents the theoretical background for the PII experiments. Section 3 presents our theoretical study of the reactive flow produced in a model elastic solid subjected to PII. Our theoretical study is presented before our experimental study because some of its results are used to interpret the longitudinal particle velocity histories recorded in the gas gun experiments. Section 4 describes the experimental methods used to fabricate the Composition B3 targets and also presents the results of the gas gun experiments. Our conclusions and recommendations are presented in Section 5.

2. THE PARALLEL-INCLINED IMPACT EXPERIMENT

2.1 EXPERIMENTAL TECHNIQUES

This section describes the techniques used to perform our compression-shear (CS) experiments in the gas gun. In these experiments, multiple Lagrange gages are used to record particle velocity histories in a target that is subjected to a parallel-inclined impact. Figure 2-1 shows a schematic view of a flyer about to strike a target in a parallel-inclined impact experiment. Upon impact, compressive and shear disturbances, parallel respectively to the directions X_1 and X_2, are produced at the impact surface because the normal to the flyer plate X_1 is not parallel to its direction of motion X_1'. These compressive and shear disturbances propagate into the target and back into the flyer and will be one-dimensional with respect to X_1 until they are influenced by lateral rarefaction waves. In a normal-impact experiment, when $\theta = 0$ and X_1 and X_1' coincide, only compressive disturbances are produced at the impact surfaces. These compressive disturbances propagate into the target and back into the flyer and will be one-dimensional with respect to X_1' until they are influenced by lateral rarefaction waves.

The Lagrange electromagnetic particle velocity (EPV) gages embedded in the target are based on the principle that an electric conductor of length $\vec{l}$ moving with a velocity $\vec{u}$ in a fixed magnetic field $\vec{B}$ will generate a motional electromotive force E given by the equation $E = \vec{l} \cdot (\vec{u} \times \vec{B})$. It follows from this equation that we can orient the magnetic field to make either longitudinal particle velocity (u_1) or shear particle velocity (u_2) measurements.

A detailed account of the experimental facility to produce and measure properties of one-dimensional compression and shear waves is given in Reference 6. A discussion of theoretical aspects of compression and shear wave propagation is presented later in this section of the report.

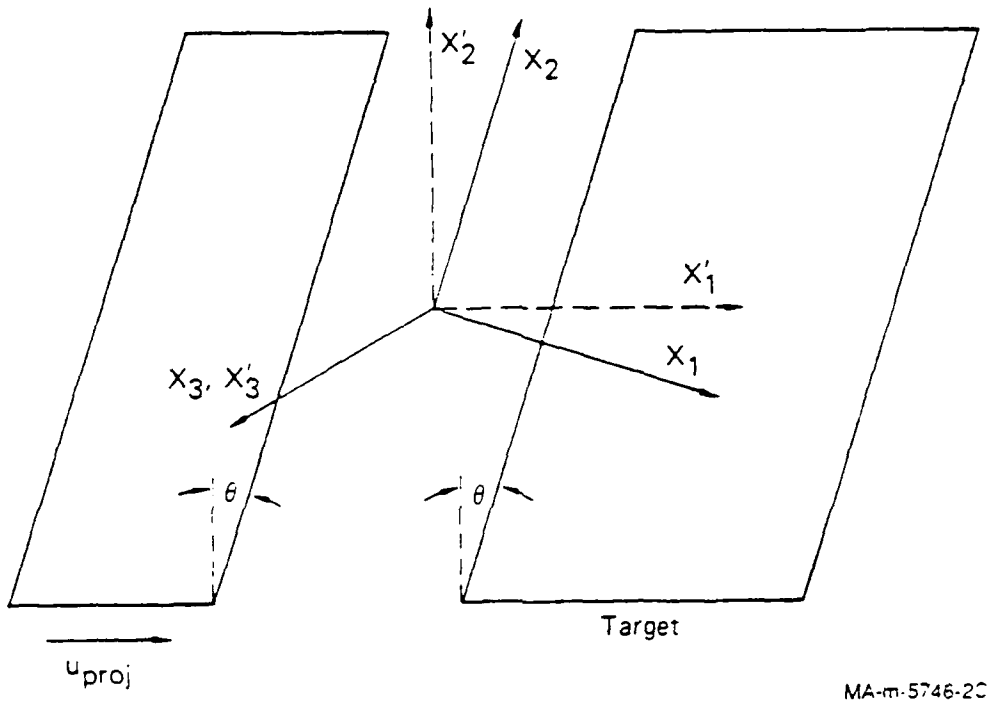

Figure 2-1. Schematic view of experimental technique to produce compression and shear waves.

The X'_i refers to the laboratory system; X_i refers to the coordinate system fixed on impact plates.

2.1.1 Compression Response

To measure compression response in a target, the angle in Figure 2-1 is set to zero in the normal impact experiments and to 15° or 20° in the PII experiments, and the magnetic field is aligned to measure $u_1(t)$. In the assembly procedure before a gas gun experiment, each target is potted in a Lucite target ring. Copper foils 2 mil thick are bonded to the impact surface across the target-Lucite interface, and copper foils 1 mil thick are bonded to the Lucite target ring. The 2-mil-thick copper foils are used to trigger the oscilloscopes in a gas gun experiment, and the 1-mil-thick copper foils are used to measure impact alignment.

The voltage signals from the EPV gages are recorded using the usual methods by analog and digital oscilloscopes. To obtain good time correlations between gages, the voltages from successive gages are recorded on fast dual-beam analog oscilloscopes (Tektronix 7844). This procedure permits an accurate determination of wave velocities and an improved analysis of the experimental data.

2.1.2 Shear Response

To measure shear response in a PII experiment, the angle θ in Figure 2-1 is set to 15° or 20° and the magnetic field is aligned so that the voltages generated by the EPV gages have only u_2 contributions. Even with good field alignment, shear particle velocity measurements are not as accurate as longitudinal particle velocity measurements. The large relative magnitude of the faster traveling longitudinal wave coupled with small errors in magnetic field alignment and impact tilt produce a small perturbation that occurs before shear wave arrival.[6] The large relative magnitude of the compression wave is a consequence of material behavior, and merely increasing θ does not produce larger shear deformation in the specimen.

The target assembly for the shear wave experiments was identical to that for the plane compression experiments.

2.2 THEORETICAL BACKGROUND

Our treatment of the PII experiment designed by Gupta[4,5] is based on the assumption that the flow produced by the impact is one-dimensional with respect to the direction normal to the plane of impact. It is convenient first to introduce the strains and stresses that are used in our analysis of the PII experiment.

2.2.1 Specification of Strain

Although we have already used X_i and X_i' to denote distances in Figure 2-1, it is convenient at this stage to introduce a new notation and let h_1, h_2, x_1, and x_2 denote, respectively, the Lagrange coordinates and the Eulerian coordinates normal and parallel to the plane of impact. In this case, to account for the fact that a particle may start to move with a velocity u_1 in the x_1 direction and a velocity u_2 in the x_2 direction at different times, we write the equations for the particle paths as

$$x_1 = h_1 + \int_{\tau_1}^{t} u_1 dt \tag{1}$$

$$x_2 = h_2 + \int_{\tau_2}^{t} u_2 dt \tag{2}$$

so that $u_1 = 0$ when $t \leq \tau_1$ and $u_2 = 0$ when $t \leq \tau_2$. Remembering that the flow is one-dimensional and that u_1 and u_2 are functions of h_1 and t, we can differentiate Equations (1) and (2) to obtain the following equations for the deformation gradients:

$$\frac{\partial x_1}{\partial h_1} = 1 + \int_{\tau_1}^{t} \frac{\partial u_1}{\partial h_1} dt$$

$$\frac{\partial x_1}{\partial h_2} = 0 \tag{3}$$

$$\frac{\partial x_2}{\partial h_1} = \int_{\tau_2}^{t} \frac{\partial u_2}{\partial h_1}\, dt$$

$$\frac{\partial x_2}{\partial h_2} = 1$$

Following the notation used by Thurston,[7] we can then write the matrix of the deformation gradients F as

$$F = \begin{pmatrix} (\partial x_1/\partial h_1), & 0 \\ (\partial x_2/\partial h_2), & 1 \end{pmatrix} \tag{4}$$

and construct a strain tensor V from the equation

$$V = \frac{1}{2}\,(C - I) \tag{5}$$

where I denotes the unit matrix, and the right Cauchy-Green tensor $C = F^{+}F$, where F^{+} is the transpose of F. We can then use the equations in (3) to obtain the elements of V describing the strain produced in our PII experiments as

$$V_{11} = \frac{1}{2}\left[\left(\frac{\partial x_1}{\partial h_1}\right)^2 + \left(\frac{\partial x_2}{\partial h_1}\right)^2 - 1\right]$$

$$V_{12} = V_{21} = \frac{1}{2}\left(\frac{\partial x_2}{\partial h_1}\right) \tag{6}$$

$$V_{22} = 0$$

It is convenient at this stage to introduce the symbol J for the determinant of F,

$$J = \det F \tag{7}$$

and present the following equations for the elements of C^{-1} that are used later in our discussion of stress in the PII experiment:

$$\frac{\partial h_1}{\partial x_1} = \frac{1}{J}\left(\frac{\partial x_2}{\partial h_2}\right) = \left(\frac{\partial x_1}{\partial h_1}\right)^{-1}$$

$$\frac{\partial h_1}{\partial x_2} = -\frac{1}{J}\left(\frac{\partial x_1}{\partial h_2}\right) = 0$$

$$\frac{\partial h_2}{\partial x_1} = -\frac{1}{J}\left(\frac{\partial x_2}{\partial h_1}\right) \qquad (8)$$

$$\frac{\partial h_2}{\partial x_2} = \frac{1}{J}\left(\frac{\partial x_1}{\partial h_1}\right) = 1$$

2.2.2 Mass Balance Equations

We recall that the mass balance equation[7] can be written in terms of the density ρ or the specific volume $v = 1/\rho$ as

$$\rho J = \rho_o, \quad v = v_o J \qquad (9)$$

where the subscript o denotes the initial state of the material. It then follows from Equations (4), (7), and (9) that the mass balance equations take the following forms for our PII experiment:

$$\rho\left(\frac{\partial x_1}{\partial h_1}\right) = \rho_o, \quad v = v_o\left(\frac{\partial x_1}{\partial h_1}\right), \quad \frac{\partial v}{\partial t} = v_o\left(\frac{\partial u_1}{\partial h_1}\right) \qquad (10)$$

2.2.3 Specification of Stress

The first and second Piola-Kirchhoff (PK) stress tensors are used in our treatment of material subjected to PII because Lagrange gages are used in the PII experiments to record particle velocity histories in the reference configuration.

The first PK stress tensor is conveniently introduced by transforming the equation for the infinitesimal force transmitted in a surface element in the present configuration with coordinates (x_1, x_2, x_3) into an equation in the reference configuration with coordinates (h_1, h_2, h_3).

To perform this transformation, we use the exterior calculus of Cartan[8] to write the equation for a surface element $d\underline{a}$ with unit normal $\underline{n}$ in the current configuration as

$$d\underline{a} = dx_1 \wedge dx_2\, e_3 + dx_2 \wedge dx_3\, e_1 + dx_3 \wedge dx_1\, e_2 = \underline{n}da \tag{11}$$

and the equation for a surface element $d\underline{A}$ with unit normal $\underline{N}$ in the initial configuration as

$$d\underline{A} = dh_1 \wedge dh_2\, e_3 + dh_2 \wedge dh_3\, e_1 + dh_3 \wedge dh_1\, e_2 = \underline{N}dA \tag{12}$$

where e_1, e_2, and e_3 are the unit vectors in the current and reference configurations.

It follows from Equations (11) and (12) that we can write

$$\begin{aligned} n_1 da &= dx_2 \wedge dx_3 \\ n_2 da &= dx_3 \wedge dx_1 \\ n_3 da &= dx_1 \wedge dx_2 \end{aligned} \tag{13}$$

$$\begin{aligned} N_1 dA &= dh_2 \wedge dh_3 \\ N_2 dA &= dh_3 \wedge dh_1 \\ N_3 dA &= dh_1 \wedge dh_2 \end{aligned} \tag{14}$$

Transforming Equation (13) into the initial configuration then leads to the equations

$$\begin{aligned} dx_1 \wedge dx_2 &= J\left(\frac{\partial h_1}{\partial x_3}\, dh_2 \wedge dh_3 + \frac{\partial h_2}{\partial x_3}\, dh_3 \wedge dh_1 + \frac{\partial h_3}{\partial x_3}\, dh_1 \wedge dh_2\right) \\ dx_2 \wedge dx_3 &= J\left(\frac{\partial h_1}{\partial x_1}\, dh_2 \wedge dh_3 + \frac{\partial h_2}{\partial x_1}\, dh_3 \wedge dh_1 + \frac{\partial h_3}{\partial x_1}\, dh_1 \wedge dh_2\right) \\ dx_3 \wedge dx_1 &= J\left(\frac{\partial h_1}{\partial x_2}\, dh_2 \wedge dh_3 + \frac{\partial h_2}{\partial x_2}\, dh_3 \wedge dh_1 + \frac{\partial h_3}{\partial x_2}\, dh_1 \wedge dh_2\right) \end{aligned} \tag{15}$$

and it follows from Equations (13) and (14) that we can express the equations in (15) by the equation

$$n_j da = J \frac{\partial h_k}{\partial x_j} N_k dA \tag{16}$$

Taking the exterior derivative of the equations in (16) also leads directly to the expression

$$\frac{\partial}{\partial h_k}\left(J \frac{\partial h_k}{\partial x_j}\right) = 0 \tag{17}$$

which is equivalent to the identity of Euler, Piola, and Jacobi.[9]

We are now in a position to introduce the first PK tensor with Cartesian coordinates P_{jk}. We first use the Cauchy stress tensor with Cartesian components σ_{ij} to write the equation for the infinitesimal force $\underline{dF}$ transmitted in a surface element $\underline{da}$ in the current configuration as

$$\underline{dF} = \sigma_{ij} n_i da e_j \tag{18}$$

We then combine Equations (15) and (16) to obtain the expression for $\underline{dF}$ in the reference configuration as

$$\underline{dF} = J \sigma_{ij} \frac{\partial h_k}{\partial x_i} N_k dA e_j \tag{19}$$

and set

$$P_{jk} = J \sigma_{ij} \frac{\partial h_k}{\partial x_i} \tag{20}$$

It follows from Equations (18) and (19) that we can compute the net j-component of force resulting from stress on a body by integrating $\sigma_{ij} n_i$ over its bounding surface in the present configuration or by integrating $P_{jk} N_k$ over its bounding surface in the reference configuration. Consequently, in the absence of body forces, the equations of motion expressing the balance of linear momentum in the current configuration,

$$\rho \frac{du_i}{dt} = - \frac{\partial \sigma_{ji}}{\partial x_j} \tag{21}$$

can be transformed into the equations of motion expressing the balance of momentum in the reference configuration,

$$\rho_o \frac{\partial u_i}{\partial t} = - \frac{\partial P_{ij}}{\partial h_j} \tag{22}$$

A consideration of the rate of work $\dot{W}$ performed at the bounding surface of a body in the current and reference configurations is used to define the second PK stress tensor. It follows from our previous discussion that $\dot{W}$ can be expressed in the current and reference configurations by the equations

$$\dot{W} = \int u_j \sigma_{ij} n_i da = \int u_j P_{jk} N_k dA \tag{23}$$

which can be transformed by the divergence theorem into the equations

$$\dot{W} = \int \left(u_j \frac{\partial \sigma_{ij}}{\partial x_i} + \sigma_{ij} \frac{\partial u_j}{\partial x_i}\right) dx_1 \wedge dx_2 \wedge dx_3 = \int \left(u_j \frac{\partial P_{jk}}{\partial h_k} + P_{jk} \frac{\partial u_j}{\partial h_k}\right) dh_1 \wedge dh_2 \wedge dh_3 \tag{24}$$

While Equations (21) and (22) show that the first terms in these integrals represent power of translation, the second terms represent power extended in stretching the material. The second PK tensor is defined, to make the equations for the stretching power per unit volume in the current and reference configurations have the same form, as follows. Because $\sigma_{ij} = \sigma_{ji}$, we first write the equation for the stretching power per unit volume in the current frame as

$$\sigma_{ij} \frac{\partial u_j}{\partial x_i} = \sigma_{ij} d_{ij} \tag{25}$$

where d_{ij} is the stretching tensor defined by the equation

$$d_{ij} = \frac{1}{2} \left(\frac{\partial u_i}{\partial x_j} + \frac{\partial u_j}{\partial x_i}\right) \tag{26}$$

We next use the equation $dx_1 \wedge dx_2 \wedge dx_3 = J\, dh_1 \wedge dh_2 \wedge dh_3$ and the identity relating d_{ij} and the rate of strain tensor $\dot{C}_{ij} = 2\dot{V}_{ij}$,[7]

$$d_{ij} = \frac{\partial h_r}{\partial x_i} \frac{\partial h_s}{\partial x_j} \dot{V}_{rs} \tag{27}$$

to obtain the equation for the stretching power per unit volume of the reference configuration as

$$J\sigma_{ij} d_{ij} = J\sigma_{ij} \frac{\partial h_r}{\partial x_i} \frac{\partial h_s}{\partial x_j} \dot{V}_{rs} \tag{28}$$

The second PK tensor is then defined as

$$T_{rs} = J\sigma_{ij} \frac{\partial h_r}{\partial x_i} \frac{\partial h_s}{\partial x_j} \tag{29}$$

to make $T_{rs}\dot{V}_{rs}$ the expression for the stretching power per unit volume in the reference configuration.

It follows from Equations (20) and (29) that the first and second PK tensors are related by the equations

$$T_{rs} = P_{jr} \frac{\partial h_s}{\partial x_j} \tag{30}$$

and

$$P_{ir} = \frac{\partial x_i}{\partial h_s} T_{rs} \tag{31}$$

We are now in a position to derive the relationships among σ_{ij}, P_{ik}, and T_{ik} in our PII experiment. The equations relating the components of the Cauchy and first PK stress tensors are obtained from Equations (20) and (13) as

$$\begin{aligned} P_{11} &= \sigma_{11} \\ P_{12} &= -\sigma_{11} \frac{\partial x_2}{\partial h_1} + J\sigma_{21} \end{aligned} \tag{32}$$

$$P_{21} = \sigma_{12} = \sigma_{21}$$

$$P_{22} = - \sigma_{12} \frac{\partial x_2}{\partial h_1} + \sigma_{22}$$

The equations relating the components of the first and second PK tensors are obtained from Equations (31) and (3) as

$$\begin{aligned} P_{11} &= \frac{\partial x_1}{\partial h_1} T_{11} \\ P_{12} &= \frac{\partial x_1}{\partial h_1} T_{21} \\ P_{21} &= \frac{\partial x_2}{\partial h_1} T_{11} + T_{12} \\ P_{22} &= \frac{\partial x_2}{\partial h_1} T_{21} + T_{22} \end{aligned} \tag{33}$$

2.2.4 Equations of Motion

It follows from Equation (21) that we can write the equations of motion in the current configuration for our one-dimensional flow produced by PII as

$$\begin{aligned} \rho \frac{du_1}{dt} &= - \frac{\partial \sigma_{11}}{\partial x_1} \\ \rho \frac{du_2}{dt} &= - \frac{\partial \sigma_{12}}{\partial x_1} \end{aligned} \tag{34}$$

The combination of Equation (34) with Equations (9) and (33) then gives the corresponding flow equations in the reference configuration [Equation (22)] as

$$\begin{aligned} \rho_o \frac{\partial u_1}{\partial t} &= - \frac{\partial P_{11}}{\partial h_1} \\ \rho_o \frac{\partial u_2}{\partial t} &= - \frac{\partial P_{21}}{\partial h_1} \end{aligned} \tag{35}$$

2.2.5 The Energy Equation and Equations of State

To complete the balance equations for our PII experiment, we assume that the flow in material subjected to PII is adiabatic. In this case, it follows from the first law of thermodynamics, with $\dot{W}$ specified by equation (23), that we can write the equations for the time rate of change of the specific internal energy e in the current and reference configurations as

$$\rho \frac{de}{dt} = - \sigma_{ij} d_{ij} \tag{36}$$

and

$$\rho_o \frac{\partial e}{\partial t} = - P_{ij} \frac{\partial u_i}{\partial h_j} \tag{37}$$

$$\rho_o \frac{\partial e}{\partial t} = - T_{ij} \dot{V}_{ij} \tag{38}$$

It then follows from Equations (37) and (38) that we can write the energy equation for our PII experiment as

$$\rho_o \frac{\partial e}{\partial t} = - P_{11} \frac{\partial u_1}{\partial h_1} - P_{21} \frac{\partial u_2}{\partial h_1} \tag{39}$$

or

$$\rho_o \frac{\partial e}{\partial t} = - T_{11} \dot{V}_{11} - T_{12} \dot{V}_{12} - T_{21} \dot{V}_{21} \tag{40}$$

To provide a more complete description of the flow, we assume that the material subjected to PII is an inert elastic solid and denote its specific entropy and temperature by s and T. The differential forms of the $e = e(s, v_o \partial x_i / \partial h_j)$ and $e = e(s, v_o V_{ij})$ equations of state (EOS)[10,7] can then be written as

$$de = Tds - v_o p_{ij} d(\partial x_i / \partial h_j) \tag{41}$$

$$de = Tds - v_o t_{ij} dV_{ij} \tag{42}$$

where $p_{ij} = -\partial e/\partial(v_o \partial x_i/\partial h_j)$ and $t_{ij} = -\partial e/\partial(v_o V_{ij})$ are the thermodynamic stresses corresponding to the first and second PK stresses. Equations (37) and (41) and Equations (38) and (42) can then be combined to give the following equations for the entropy production in adiabatic, nonreactive flow.

$$T \frac{\partial s}{\partial t} = - v_o (P_{ij} - p_{ij}) \frac{\partial u_i}{\partial h_j} \tag{43}$$

$$T \frac{\partial s}{\partial t} = - v_o (T_{ij} - t_{ij}) \dot{V}_{ij} \tag{44}$$

Equations (43) and (44) are expressions of the second law of thermodynamics for the adiabatic flow of an inert elastic solid. To simplify our treatment of the adiabatic flow in a reactive elastic solid, we will assume that the entropy production is dominated by the reaction and accordingly set $P_{ij} = p_{ij}$ and $T_{ij} = t_{ij}$ in regions free from shocks.

2.3 IDEAL INERT FLOW PRODUCED BY PARALLEL-INCLINED IMPACT

Our analysis of the ideal flow produced in a PII experiment is based on the assumption that inert material subjected to PII can support two waves, a compression wave (CW) in which $\partial u_2/\partial t = 0$ and a subsequent shear wave (SW) in which $\partial u_1/\partial t = 0$. The conditions required to obtain this type of flow are formulated later in this report.

2.3.1 Flow in the Pure Compression Wave

When $\partial u_2/\partial t = 0$ in the CW, we use the identities

$$u_2 = \int_{\tau_1}^{t} \frac{\partial u_2}{\partial t} \, dt \tag{45}$$

$$\frac{\partial u_2}{\partial h_1} = \int_{\tau_1}^{t} \frac{\partial^2 u_2}{\partial h_1 \partial t} \, dt \tag{46}$$

to show that $u_2 = 0$ and $\partial u_2/\partial h_1 = 0$. It then follows from Equations (3), (6), (33), (35), and the equation

$$P_{21} = \int_{h_{if}}^{h_1} \frac{\partial P_{21}}{\partial h_1}\, dh_1 = -\rho_o \int_{h_{if}}^{h_1} \frac{\partial u_2}{\partial t}\, dh_1 \tag{47}$$

that the flow in the CW also satisfies the equations

$$\frac{\partial x_2}{\partial h_1} = 0 \tag{48}$$

$$V_{11} = \frac{1}{2}\left[\left(\frac{\partial x_1}{\partial h_1}\right)^2 - 1\right] \tag{49}$$

$$V_{12} = V_{21} = 0 \tag{50}$$

$$P_{21} = T_{12} = 0 \tag{51}$$

We will now perform a Lagrange analysis with the mass balance and momentum equations,

$$\frac{\partial v}{\partial t} = v_o \frac{\partial u_1}{\partial h_1} \tag{52}$$

$$\rho_o \frac{\partial u_1}{\partial t} = -\frac{\partial P_{11}}{\partial h_1} \tag{53}$$

to determine stress-strain conditions for a CW to form a shock and propagate at a constant velocity. Extending the notation introduced by Fowles,[11,12] we set $(\partial h_1/\partial t)u_1 = C_1$ and rewrite Equations (52) and (53) in integral form as

$$v - v_o = v_o \int_{\tau_1}^{t} \frac{\partial u_1}{\partial h_1}\, dt = -v_o \int_0^{u_1} C_1^{-1} du_1 \tag{54}$$

$$P_{11} = -\rho_o \int_{h_{if}}^{h_1} \frac{\partial u_1}{\partial t}\, dh_1 = \rho_o \int_0^{u_1} C_1 du_1 \tag{55}$$

Differentiating Equation (54) with respect to h_1 at constant u_1 and Equation (55) with respect to t at constant u_1 then leads to the equations

$$\left(\frac{\partial v}{\partial h_1}\right)_{u_1} = - v_o \int_0^{u_1} \left(\frac{\partial^2 t}{\partial h_1^2}\right)_{u_1} du_1 \tag{56}$$

$$\left(\frac{\partial P_{11}}{\partial t}\right)_{u_1} = \rho_o \int_0^{u_1} \left(\frac{\partial^2 h_1}{\partial t^2}\right)_{u_1} du_1 \tag{57}$$

which show that $v = v(u_1)$ and $P_{11} = P_{11}(u_1)$ when $C_1 = C_1(u_1)$.

We now consider such a simple wave with $C_1 = C_1(u_1)$. We rewrite Equations (52) and (53) as

$$\frac{du_1}{d(\partial x_1/\partial h_1)} = - C_1 \tag{58}$$

$$\frac{dP_{11}}{du_1} = \rho_o C_1 \tag{59}$$

and then combine Equations (58) and (59) to obtain the equation

$$\frac{dP_{11}}{d(\partial x_1/\partial h_1)} = - \rho_o C_1^2 \tag{60}$$

which relates the slope of the first PK stress-strain curve in the reference configuration to the square of the propagation velocity C_1. It follows from Equation (60) that the slope of the stress (P_{11}) - strain ($\partial x_1/\partial h_1$) curve is negative. Differentiation of equation (60) with respect to u_1 then gives the equation

$$\frac{dC_1}{du_1} = \frac{v_o}{2C_1^2} \frac{d^2 P_{11}}{d(\partial x_1/\partial h_1)^2} \tag{61}$$

which can be used to derive conditions for a simple CW to steepen, flatten, or remain unchanged as it propagates. We now note that $dC_1/du_1 > 0$ is the condition for a simple CW to steepen, $dC_1/du_1 < 0$ the

condition for a simple CW to flatten, and $dC_1/du_1 = 0$ is the condition for a simple CW to propagate unchanged. It then follows from Equation (61) that a simple CW will steepen to form a shock if $d^2P_{11}/d(\partial x_1/\partial h_1)^2 > 0$, will flatten and spread out if $d^2P_{11}/d(\partial x_1/\partial h_1)^2 < 0$, and will propagate unchanged if $d^2P_{11}/d(\partial x_1/\partial h_1)^2 = 0$.

We now use Equations (33) and (49) to formulate these conditions in terms of the relationship between the second PK stress and the V_{11} strain as follows. Differentiating Equations (33) and (49) leads to the equations

$$\frac{dP_{11}}{d(\partial x_1/\partial h_1)} = T_{11} + \left(\frac{\partial x_1}{\partial h_1}\right)^2 \frac{dT_{11}}{dV_{11}} = -\rho_o C_1^2 \tag{62}$$

and

$$\frac{d^2P_{11}}{d(\partial x_1/\partial h_1)^2} = 3\left(\frac{\partial x_1}{\partial h_1}\right)\frac{dT_{11}}{dV_{11}} + \left(\frac{\partial x_1}{\partial h_1}\right)^3 \frac{d^2T_{11}}{dV_{11}^2} \tag{63}$$

It follows from Equation (62), because $T_{11} \geq 0$ and $dT_{11}/dV_{11} < 0$, that the $(T_{11} - V_{11})$ stress-strain curve must satisfy the condition $|dT_{11}/dV_{11}| > T_{11}(\partial h_1/\partial x_1)^2$. It also follows from Equation (63) that conditions for shock formation are more complicated when they are expressed in terms of the $(T_{11} - V_{11})$ curve rather than the $(P_{11} - \partial x_1/\partial h_1)$ curve because the condition $d^2P_{11}/d(\partial x_1/\partial h_1)^2 > 0$ ensures shock formation in a simple CW but the condition $d^2T_{11}/dV_{11}^2 > 0$ does not.

Steady-State Flow. We now consider the situation when the CW attains a steady-state and propagates unchanged with a velocity D. In this case, because $dC_1/du_1 = 0$, we can set $C_1 = D$ and integrate Equations (58), (59), and (60) to obtain the Rankine-Hugoniot jump conditions

$$u_1 = D\left(1 - \left(\frac{\partial x_1}{\partial h_1}\right)\right) \tag{64}$$

$$P_{11} = \rho_o D u_1 \tag{65}$$

$$P_{11} = \rho_o D^2 \left(1 - \left(\frac{\partial x_1}{\partial h_1}\right)\right) \tag{66}$$

We can then use the following equation obtained from Equations (49) and (33)

$$P_{11} = \left(2V_{11} + 1\right)^{1/2} T_{11} \tag{67}$$

to express Equations (65) and (66) in terms of the second PK stress tensor as

$$T_{11} = \rho_o Du_1 \left(2V_{11} + 1\right)^{-1/2} \tag{68}$$

$$T_{11} = \rho_o D^2 \left(\left(2V_{11} + 1\right)^{-1/2} - 1\right) \tag{69}$$

We can then use Equation (66) to integrate the energy equation

$$\rho_o \frac{\partial e}{\partial t} = - P_{11} \frac{\partial u_1}{\partial h_1} \tag{70}$$

to obtain the Hugoniot relation

$$e - e_o = \frac{1}{2} v_o P_{11} \left(1 - \frac{\partial x_1}{\partial h_1}\right) \tag{71}$$

which is readily transformed into the equation

$$e - e_o = \frac{v_o}{2} T_{11} \left(\left(2V_{11} + 1\right)^{1/2} - \left(2V_{11} + 1\right)\right) \tag{72}$$

Thermodynamic Considerations. We are now in a position to use the $e = e(s, v_o \partial x_i/\partial h_j)$ and $e = e(s, v_o V_{ij})$ EOS to consider thermodynamics aspects of the flow. At this stage, for convenience in writing partial derivatives, we set $\partial x_1'/\partial h_1 = x_1'$ and $\partial x_2/\partial h_1 = x_2'$. For this purpose, it is convenient to discuss the isentropic, simple CW. In this case, we can set $P_{ij} = p_{ij}$ and $T_{ij} = t_{ij}$ in Equations (43) and (44), rewrite Equations (60) and (61) as

$$\left(\frac{\partial p_{11}}{\partial (\partial x_1/\partial h_1)}\right)_{s, x_2'} = - \rho_o C_1^2 \tag{73}$$

$$\frac{dC_1}{du_1} = \frac{v_o}{2C_1^2}\left(\frac{\partial^2 p_{11}}{\partial\left(\partial x_1/\partial h_1\right)^2}\right)_{s,x_2'} \tag{74}$$

and Equations (62) and (63) as

$$t_{11} + (2V_{11} + 1)\left(\frac{\partial t_{11}}{\partial V_{11}}\right)_{s,V_{12},V_{21}} = -\rho_o C_1^2 \tag{75}$$

$$\left(\frac{\partial^2 p_{11}}{\partial(\partial x_1/\partial h_1)^2}\right)_{s,x_2'} = 3(2V_{11} + 1)^{1/2}\left(\frac{\partial t_{11}}{\partial V_{11}}\right)_{s,V_{12},V_{21}} + (2V_{11} + 1)^{3/2}\left(\frac{\partial^2 t_{11}}{\partial V_{11}^2}\right)_{s,V_{12},V_{21}} \tag{76}$$

where $(\partial t_{11}/\partial V_{11})_{s,V_{12}}$ and $(\partial^2 t_{11}/\partial V_{11}^2)_{s,V_{12}}$ are respectively called the second-order and third-order isentropic elastic stiffness coefficients. Equations (10) and (35), written for isentropic flow, can then be combined to show that the slopes of the characteristics in the $(t - h_1)$ plane are given by the equation

$$\frac{dh_1}{dt} = \pm\left(-v_o\left(\frac{\partial p_{11}}{\partial(\partial x_1/\partial h_1)}\right)_{s,x_2'}\right)^{1/2} \tag{77}$$

and it then follows from Equation (73) that, in a simple isentropic CW, the lines of constant particle velocity in the $(t - h_1)$ plane are also the forward facing characteristics. Equation (74) for the change in the slopes of the lines of constant particle velocity with particle velocity is thus equivalent to the equation given by Courant and Friedrichs[13] for the change in the slopes of the characteristics with particle velocity for a fluid. In this light, it is clear that C_1 can be calculated in our simple isentropic CW with $\partial x_2/\partial h_1 = 0$ from the $e = e(p_{11}, v_o x_1', v_o x_2')$ EOS as follows. Equating the expressions for de obtained from the $e = e(s, v_o x_1', v_o x_2')$ and $e = e(p_{11}, v_o x_1', v_o x_2')$ EOS leads to the equation

$$Tds - p_{11}d(v_o(\partial x_1/\partial h_1) = \left(\frac{\partial e}{\partial p_{11}}\right)_{x_1',x_2'} dp_{11}$$

$$+ \left(\frac{\partial e}{\partial(v_o\partial x_1/\partial h_1)}\right)_{p_{11},x_2'} d\left(v_o(\partial x_1/\partial h_1)\right) \quad (78)$$

which reduces to the following equation when ds = 0:

$$\left(\frac{\partial p_{11}}{\partial(\partial x_1/\partial h_1)}\right)_{s,x_2'} = - v_o\left(\frac{p_{11} + \left(\partial e/\partial(v_o\partial x_1/\partial h_1)\right)_{p_{11},x_2'}}{(\partial e/\partial p_{11})_{x_1',x_2'}}\right) \quad (79)$$

When the $e = e(p_{11},v_ox_1',v_ox_2')$ EOS is known, Equation (79) can be integrated to obtain the $(p_{11} - \partial x_1/\partial h_1)$ expression for an isentrope, and then Equations (73) and (74) can be used to calculate values of C_1 and the corresponding values of dC_1/du_1.

We finally consider equations (73, (75), (76), and (79). First, we note that Equation (79) can be transformed into Equation (75) by making use of the equations

$$\left(\frac{\partial e}{\partial p_{11}}\right)_{x_1',x_2'} = \left(\frac{\partial x_1}{\partial h_1}\right)^{-1}\left(\frac{\partial e}{\partial t_{11}}\right)_{V_{11},V_{12},V_{21}} \quad (80)$$

$$\left(\frac{\partial e}{\partial(v_o\,\partial x_1/\partial h_1)}\right)_{p_{11},x_2'} = \left(\frac{\partial x_1}{\partial h_1}\right)\left(\frac{\partial e}{\partial(v_oV_{11})}\right)_{t_{11},V_{12},V_{21}}$$

$$- \frac{t_{11}}{v_o}\left(\frac{\partial e}{\partial p_{11}}\right)_{x_1',x_2'} \quad (81)$$

$$\left(\frac{\partial t_{11}}{\partial V_{11}}\right)_{s,V_{12},V_{21}} = - v_o\frac{\left[t_{11} + \left(\partial e/\partial(v_oV_{11})\right)_{t_{11},V_{12},V_{21}}\right]}{(\partial e/\partial t_{11})_{V_{11},V_{12},V_{21}}} \quad (82)$$

We next note, from Equations (73) and (75), that the initial slopes of the $(p_{11} - \partial x_1/\partial h_1)$ and $(t_{11} - V_{11})$ isentropes are the same and define the propagation velocity of the foot of a simple isentropic CW. Finally,

we note from Equation (76) that model elastic solids that do not include third-order isentropic elastic stiffness coefficients in the formulation of their $e = e(s, v_o V_{ij})$ EOS will not support the propagation of a compressive shock because $(\partial t_{11}/\partial V_{11})_{s,V_{12},V_{21}} < 0$.

2.3.2 Flow in the Pure Shear Wave

Our treatment of the inert pure SW parallels our treatment of the CW and is based on the assumption that the CW has attained a steady state with the peak values $\hat{v} = v_o(\partial \hat{x}_1/\partial h_1)$, $\hat{u}_1$, $\hat{P}_{11} = \hat{p}_{11}$, $\hat{T}_{11} = \hat{t}_{11}$, and $\hat{e}$. When $\partial u_1/\partial t = 0$ in the SW, we use the identities

$$u_1 - \hat{u}_1 = \int_{\tau_2}^{t} \frac{\partial u_1}{\partial t}\, dt \tag{83}$$

$$\frac{\partial u_1}{\partial h_1} = \int_{\tau_2}^{t} \frac{\partial^2 u_1}{\partial h_1 \partial t}\, dt \tag{84}$$

to show that $u_1 = \hat{u}_1$ and $\partial u_1/\partial h_1 = 0$. It then follows from Equations (3), (6), (33), and (35) and the equation

$$P_{11} - \hat{P}_{11} = \int_{h'_{1f}}^{h_1} \frac{\partial P_{11}}{\partial h_1}\, dh_1 = -\rho_o \int_{h'_{1f}}^{h_1} \frac{\partial u_1}{\partial t}\, dh_1 \tag{85}$$

that

$$\frac{\partial x_1}{\partial h_1} = \frac{\partial \hat{x}_1}{\partial h_1} = \frac{\hat{v}}{v_o} \tag{86}$$

$$V_{11} = \frac{1}{2}\left[\left(\frac{\partial \hat{x}_1}{\partial h_1}\right)^2 + \left(\frac{\partial x_2}{\partial h_1}\right)^2 - 1\right] \tag{87}$$

$$V_{12} = V_{21} = \frac{1}{2}\left(\frac{\partial x_2}{\partial h_1}\right) \tag{88}$$

$$P_{11} = \hat{P}_{11} = \hat{p}_{11} \tag{89}$$

$$T_{11} = \hat{T}_{11} = \hat{t}_{11} = \hat{p}_{11} \left(\frac{\partial \hat{x}_1}{\partial h_1} \right)^{-1} \tag{90}$$

We now assume that the SW is a simple wave and write the equations

$$\frac{\partial}{\partial t} \frac{\partial x_2}{\partial h_1} = \frac{\partial u_2}{\partial h_1} \tag{91}$$

$$\rho_o \frac{\partial u_2}{\partial t} = - \frac{\partial P_{21}}{\partial h_1} \tag{92}$$

in terms of $(\partial h_1/\partial t)_{u_2} = C_2 = C_2(u_2)$ as

$$\frac{du_2}{d(\partial x_2/\partial h_1)} = - C_2 \tag{93}$$

$$\frac{dP_{21}}{du_2} = \rho_o C_2 \tag{94}$$

Following our previous discussion of the CW, we can then write

$$\frac{dP_{21}}{d(\partial x_2/\partial h_1)} = - \rho_o C_2^2 \tag{95}$$

$$\frac{dC_2}{du_2} = \frac{v_o}{2C_2^2} \frac{d^2 P_{21}}{d(\partial x_2/\partial h_1)^2} \tag{96}$$

It then follows from Equations (95) and (96) that the slope of the $(P_{21} - \partial x_2/\partial h_1)$ curve must be negative and that the SW will form a shock if $d^2P_{21}/d(\partial x_2/\partial h_1)^2 > 0$, flatten and spread if $d^2P_{21}/d(\partial x_2/\partial h_1)^2 < 0$, and propagate unchanged if $d^2P_{21}/d(\partial x_2/\partial h_1)^2 = 0$.

We now use Equation (88) and the equation from (33)

$$P_{21} = \frac{\partial x_2}{\partial h_1} \hat{T}_{11} + T_{12} \tag{97}$$

to express Equations (95) and (96) in terms of the components of the second PK stress tensor. Differentiating Equation (97) twice with respect to $(\partial x_2/\partial h_1)$ gives the equations

$$\frac{dP_{21}}{d(\partial x_2/\partial h_1)} = \hat{T}_{11} + \frac{1}{2}\frac{dT_{12}}{dV_{12}} = -\rho_o C_2^2 \tag{98}$$

$$\frac{d^2P_{21}}{d(\partial x_2/\partial h_1)^2} = \frac{1}{4}\frac{d^2T_{12}}{dV_{12}^2} \tag{99}$$

We now consider Equations (96), (97), (98), and (99). Because $(\partial x_2/\partial h_1) < 0$, it follows from Equation (97) that the condition $T_{12} > -\hat{T}_{11}(\partial x_2/\partial h_1)$ is satisfied in the SW. Because $\hat{T}_{11} > 0$, it follows from Equation (98) that $dT_{12}/dV_{12} < 0$ and also that the condition $-dT_{12}/dV_{12} > 2\hat{T}_{11}$ is satisfied in the SW. It follows as a consequence of the latter condition that the shear strain will be located close to the impact surface if $-dT_{12}/dV_{12} \sim 2\hat{T}_{11}$. It follows from Equations (96) and (99) that the tendency for a SW to steepen, flatten, or propagate unchanged is determined solely by the sign of the second derivative of the $(T_{12} - V_{12})$ stress-strain curve. It is clear that the conditions for steepening, flattening, and propagating unchanged are, respectively, $d^2T_{12}/dV_{12}^2 > 0$, $d^2T_{12}/dV_{12}^2 < 0$, and $d^2T_{12}/dV_{12}^2 = 0$.

Steady State Flow. We will now derive the equations for a shear shock, although a previous study[6] leads us to expect that solids satisfy the condition $d^2T_{12}/dV^2{}_{12} < 0$. When $d^2T_{12}/dV_{12} = 0$, we can set $C_2 = D_s$ and integrate Equation (98) to obtain the equations

$$P_{21} = -\rho_o\left(\frac{\partial x_2}{\partial h_1}\right)D_s^2 \tag{100}$$

$$T_{12} = -\rho_o 2V_{12}\left(D_s^2 + D^2\left(\frac{V_o}{\hat{V}} - 1\right)\right) \tag{101}$$

We can then use Equation (100) to integrate the energy equation

$$\rho_o\frac{\partial e}{\partial t} = -P_{21}\frac{\partial u_2}{\partial h_1} \tag{102}$$

to obtain the equation

$$e - \hat{e} = - \frac{v_o}{2} P_{21} \left(\frac{\partial x_2}{\partial h_1}\right) \tag{103}$$

which can be rewritten as

$$\hat{e} = e_o + \frac{v_o}{2} \hat{T}_{11}\left[(2\hat{V}_{11} + 1)^{1/2} - (2\hat{V}_{11} + 1)\right] - v_o V_{12}\left[2V_{12}\hat{T}_{11} + T_{12}\right] \tag{104}$$

Thermodynamic Considerations. Following our previous discussion of the CW, we will consider an isentropic, simple SW. Then we can set $P_{ij} = p_{ij}$, $T_{ij} = t_{ij}$ and rewrite Equations (95) and (96) and (97) as

$$\frac{\partial p_{21}}{\partial(\partial x_2/\partial h_1)_{s,x_1'}} = - \rho_o C_2^2 \tag{105}$$

$$\frac{dC_2}{du_2} = \frac{v_o}{2C_2^2}\left(\frac{\partial^2 p_{21}}{\partial(\partial x_2/\partial h_1)^2}\right)_{s,x_1'} \tag{106}$$

$$p_{21} = \left(\frac{\partial x_2}{\partial h_1}\right) \hat{t}_{11} + t_{12} \tag{107}$$

It then follows by differentiating Equation (107) and taking account of Equation (87) that Equations (98) and (99) can be rewritten as

$$\hat{t}_{11} + 2V_{12}\left(\frac{\partial t_{12}}{\partial V_{11}}\right)_{s,V_{12},V_{21}} + \left(\frac{\partial t_{12}}{\partial V_{12}}\right)_{s,V_{11},V_{21}} = - \rho_o C_2^2 \tag{108}$$

$$\left(\frac{\partial^2 p_{21}}{\partial(\partial x_2/\partial h_1)^2}\right)_{s,x_1'} = \left(\frac{\partial t_{12}}{\partial V_{11}}\right)_{s,V_{12},V_{21}} + \left(\frac{\partial^2 t_{12}}{\partial V_{12}^2}\right)_{s,V_{11},V_{21}}$$

$$+ 4V_{12}^2\left(\frac{\partial^2 t_{12}}{\partial V_{11}^2}\right)_{s,V_{12},V_{21}} + 4V_{12}\left(\frac{\partial^2 t_{12}}{\partial V_{11}\partial V_{12}}\right)_{s,V_{21}} \tag{109}$$

Now because $V_{12} < 0$, $(\partial t_{12}/\partial V_{11})_{s,V_{12},V_{21}} < 0$, and $(\partial t_{12}/\partial V_{12})_{s,V_{11},V_{21}} < 0$, it follows from Equation (108) that the condition $-(\partial t_{12}/\partial V_{12}) > \hat{t}_{11} + 2V_{12}(\partial t_{12}/\partial V_{11})_{s,V_{12},V_{21}}$ is satisfied in a simple isentropic SW. Comparing Equations (109) and (77) shows that the expression for the second derivative of p_{21} with respect to $(\partial x_2/\partial h_1)$ is more complicated than the expression for the second derivative of p_{11} with respect to $(\partial x_1/\partial h_1)$. This difference obviously arises because V_{11} is only a function of $(\partial x_1/\partial h_1)$ in the CW but V_{11} and V_{12} are both functions of $(\partial x_2/\partial h_1)$ in the SW. It also follows from Equation (109) that model elastic solids that do not include third-order, isentropic, elastic stiffness coefficients in the formulation of their $e = e(s, v_o V_{ij})$ EOS will support a spreading SW if $(\partial t_{12}/\partial V_{11})_{s,V_{12},V_{21}} \neq 0$ but a steady-state SW if $(\partial t_{12}/\partial V_{11}) = 0$.

The combination of Equation (92), written for isentropic flow, with Equation (91) gives the following equation for the slopes of the characteristics in the $(t - h_1)$ plane,

$$\frac{dh_1}{dt} = \pm \left(-v_o \frac{\partial p_{21}}{\partial (\partial x_2/\partial h_1)_{s,x_1'}} \right)^{1/2} \tag{110}$$

Comparing Equations (105) and (110) then shows that, in a simple isentropic SW, the lines of constant particle velocity in the $(t - h_1)$ plane are also the forward facing characteristics. From an argument similar to that presented earlier, it then follows that the differential equation for the $(p_{21} - \partial x_2/\partial h_1)$ isentropes can be written in terms of the $e = e(p_{21}, v_o \partial x_1/\partial h_1, v_o \partial x_2/\partial h_1)$ EOS as

$$\left(\frac{\partial p_{21}}{\partial (\partial x_2/\partial h_1)} \right)_{s,x_1'} = - v_o \left[\frac{p_{21} + (\partial e/\partial v_o \partial x_2/\partial h_1)_{p_{21},x_1'}}{(\partial e/\partial p_{21})_{x_1',x_2'}} \right] \tag{111}$$

Equation (111) can then be transformed into Equation (108) by making use of Equation (105) and the thermodynamic identities

$$\left(\frac{\partial e}{\partial t_{12}}\right)_{V_{11},V_{12},V_{21}} = \left(\frac{\partial e}{\partial p_{21}}\right)_{x_1',x_2'} \tag{112}$$

$$\left(\frac{\partial e}{\partial v_o \partial x_2/\partial h_1}\right)_{p_{21},x_1'} = \left(\frac{\partial x_2}{\partial h_1}\right)\left(\frac{\partial e}{\partial v_o V_{11}}\right)_{t_{12},V_{12},V_{21}}$$

$$+ \left(\frac{\partial e}{\partial v_o V_{12}}\right)_{t_{12},V_{11},V_{21}} - \frac{\hat{t}_{11}}{v_o}\left(\frac{\partial e}{\partial t_{12}}\right)_{V_{11},V_{12},V_{21}} \tag{113}$$

$$\left(\frac{\partial t_{12}}{\partial V_{11}}\right)_{s,V_{12},V_{21}} = - v_o \frac{\left[t_{11} + (\partial e/\partial v_o V_{11})_{t_{12},V_{12},V_{21}}\right]}{(\partial e/\partial p_{21})_{x_1',x_2'}} \tag{114}$$

$$\left(\frac{\partial t_{12}}{\partial V_{12}}\right)_{s,V_{11},V_{21}} = - v_o \frac{\left[t_{12} + (\partial e/\partial v_o V_{12})_{t_{12},V_{11},V_{21}}\right]}{(\partial e/\partial p_{21})_{x_1',x_2'}} \tag{115}$$

3. THEORETICAL STUDY OF REACTIVE FLOWS PRODUCED IN AN ELASTIC SOLID BY NORMAL AND PARALLEL-INCLINED IMPACT

Up to this point in our theoretical treatment, we have assumed that the flow produced in material subject to normal or parallel-inclined impact is nonreactive. To remove this restriction, we need to formulate an EOS for a reactive mixture and then combine this EOS with the energy equation to determine how the reaction influences the flow.

3.1 EQUATION OF STATE FOR A REACTIVE EXPLOSIVE MIXTURE

The formulation of an EOS for a reactive mixture of an explosive and its products is a complicated and controversial problem. We here consider the simplest case by assuming that the explosive undergoes a global decomposition to produce solid reaction products and a reactive mixture that is in thermal and mechanical equilibrium and obeys the following mixture rules for the specific internal energy, the specific entropy, and the strain, respectively:

$$e = (1 - \lambda)e_x + \lambda e_p \tag{116}$$

$$s = (1 - \lambda)s_x + \lambda s_p \tag{117}$$

$$v_o \frac{\partial x_i}{\partial h_j} = (1 - \lambda)v_o^x \frac{\partial x_i}{\partial h_j} + \lambda v_o^p \frac{\partial x_i}{\partial h_j} \tag{118}$$

In these equations, we use the subscripts and superscripts x and p to denote the explosive and its products, and we use λ to denote the mass fraction of explosive that has decomposed. We now let Q denote the standard heat of decomposition of the explosive, rewrite the specific energies of the explosive and its products as

$$e_x = e_x^o + \tilde{e}_x\left(s_x, v_o^x(\partial x_i/\partial h_j)^x\right) \tag{119}$$

$$e_p = -Q + e_x^o + \tilde{e}_p\left(s_p, v_o^p(\partial x_i/\partial h_j)^p\right) \tag{120}$$

and combine Equations (116), (119), and (120) to obtain the equation

$$e = e_x^o - \lambda Q + (1 - \lambda)\tilde{e}_x + \lambda\tilde{e}_p \tag{121}$$

We next combine the differential forms obtained from Equations (121), (117), and (118) with Equation (41) written for the explosive and its products and the equilibrium conditions, $T_x = T_p$ and $p_{ij}^x = p_{ij}^p$, to obtain the following differential form expressing e as a function of s, $\partial x_i/\partial h_j$, and λ:

$$de = Tds - v_o p_{ij} d(\partial x_i/\partial h_j) - Ad\lambda \tag{122}$$

where

$$A = \lambda Q + \left[\tilde{e}_x - Ts_x + p_{ij}\left(\frac{\partial x_i}{\partial h_j}\right)^x - \left(\tilde{e}_p - Ts_p + p_{ij}\left(\frac{\partial x_i}{\partial h_j}\right)^p\right)\right] \tag{123}$$

At this stage, we have shown that a reactive explosive mixture obeying our assumptions can be described by an $e = e(s, v_o \partial x_i/\partial h_j, \lambda)$ EOS. We must now combine Equation (122) with the flow equations to obtain the corresponding thermodynamic equations governing reactive flow.

3.2 THERMODYNAMICS OF THE REACTIVE FLOW OF AN ELASTIC SOLID

Our derivation of the thermodynamic equations governing the adiabatic reactive flow of an elastic solid is based on the ZND assumption[14] that the entropy production in regions free from shocks is associated solely with the chemical reaction. In this case, we can set $P_{ij} = p_{ij}$, as discussed previously, and combine Equation (39) with Equation (122) written as

$$\frac{\partial e}{\partial t} = T\frac{\partial s}{\partial t} - v_o P_{11}\frac{\partial u_1}{\partial h_1} - v_o P_{21}\frac{\partial u_2}{\partial h_1} - A\frac{\partial \lambda}{\partial t} \tag{124}$$

to obtain the basic equation governing our reactive flow

$$\frac{\partial s}{\partial t} = \frac{A}{T}\frac{\partial \lambda}{\partial t} = \left(\frac{\partial s}{\partial \lambda}\right)_{e,x_1',x_2'} \frac{\partial \lambda}{\partial t} \tag{125}$$

The combination of equation (125) with the $s = s(p_{11}, v_o x_1', v_o x_2', \lambda)$ and $s = s(p_{21}, v_o x_1', v_o x_2', \lambda)$ EOS then leads to the equations

$$\frac{\partial p_{11}}{\partial t} = \left(\frac{\partial p_{11}}{\partial x_1'}\right)_{s,x_2',\lambda} \frac{\partial u_1}{\partial h_1} + \left(\frac{\partial p_{11}}{\partial x_2'}\right)_{s,x_1',\lambda} \frac{\partial u_2}{\partial h_1} + \left(\frac{\partial p_{11}}{\partial \lambda}\right)_{e,x_1',x_2'} \frac{\partial \lambda}{\partial t} \tag{126}$$

$$\frac{\partial p_{21}}{\partial t} = \left(\frac{\partial p_{21}}{\partial x_1'}\right)_{s,x_2',\lambda} \frac{\partial u_1}{\partial h_1} + \left(\frac{\partial p_{21}}{\partial x_2'}\right)_{s,x_1',\lambda} \frac{\partial u_2}{\partial h_1} + \left(\frac{\partial p_{21}}{\partial \lambda}\right)_{e,x_1',x_2'} \frac{\partial \lambda}{\partial t} \tag{127}$$

where

$$\left(\frac{\partial p_{11}}{\partial \lambda}\right)_{e,x_1',x_2'} = \left(\frac{\partial p_{11}}{\partial \lambda}\right)_{s,x_1',x_2'} + \left(\frac{\partial p_{11}}{\partial s}\right)_{\lambda,x_1',x_2'} \frac{A}{T} = -\frac{(\partial e/\partial \lambda)_{p_{11},x_1',x_2'}}{(\partial e/\partial p_{11})_{x_1',x_2',\lambda}} \tag{128}$$

and

$$\left(\frac{\partial p_{21}}{\partial \lambda}\right)_{e,x_1',x_2'} = \left(\frac{\partial p_{21}}{\partial \lambda}\right)_{s,x_1',x_2'} + \left(\frac{\partial p_{21}}{\partial s}\right)_{\lambda,x_1',x_2'} \frac{A}{T} = \frac{(\partial e/\partial \lambda)_{p_{21},x_1',x_2'}}{(\partial e/\partial p_{21})_{x_1',x_2',\lambda}} \tag{129}$$

Combining Equation (126) with the $T = T(p_{11}, v_o x_1', v_o x_2', \lambda)$ EOS and Equation (127) with the $T = T(p_{21}, v_o x_1', v_o x_2', \lambda)$ EOS leads to the equations

$$\left(\frac{\partial p_{11}}{\partial T}\right)_{x_1',x_2',\lambda} \frac{\partial T}{\partial t} = \left(\frac{\partial p_{11}}{\partial x_1'}\right)_{s,x_2',\lambda} \left(1 - \frac{C_{x_1',x_2',\lambda}}{C_{p_{11},x_2',\lambda}}\right) \frac{\partial u_1}{\partial h_1}$$

$$+ \left(\frac{\partial p_{11}}{\partial x_2'}\right)_{s,x_1',\lambda} \left(1 - \frac{C_{x_1',x_2',\lambda}}{C_{p_{11},x_1',\lambda}}\right) \frac{\partial u_2}{\partial h_1} + \left[\left(\frac{\partial p_{11}}{\partial \lambda}\right)_{e,x_1',x_2'} - \left(\frac{\partial p_{11}}{\partial \lambda}\right)_{T,x_1',x_2'}\right] \frac{\partial \lambda}{\partial t} \tag{130}$$

$$\left(\frac{\partial p_{21}}{\partial T}\right)_{x_1',x_2',\lambda} \frac{\partial T}{\partial t} = \left(\frac{\partial p_{21}}{\partial x_1'}\right)_{s,x_2',\lambda} \left(1 - \frac{C_{x_1',x_2',\lambda}}{C_{p_{21},x_2',\lambda}}\right) \frac{\partial u_1}{\partial h_1}$$

$$+ \left(\frac{\partial p_{21}}{\partial x_2'}\right)_{s,x_1',\lambda} \left(1 - \frac{C_{x_1',x_2',\lambda}}{C_{p_{21},x_1',\lambda}}\right) \frac{\partial u_2}{\partial h_1} + \left[\left(\frac{\partial p_{21}}{\partial \lambda}\right)_{e,x_1',x_2'} - \left(\frac{\partial p_{21}}{\partial \lambda}\right)_{T,x_1',x_2'}\right] \frac{\partial \lambda}{\partial t} \tag{131}$$

where the specific heats $C_{x_1',x_2',\lambda}$ and $C_{p_{ij},x_k',\lambda}$ are defined by the equations

$$C_{x_1',x_2',\lambda} = T \left(\frac{\partial s}{\partial T}\right)_{x_1',x_2',\lambda} \tag{132}$$

$$C_{p_{ij},x_k',\lambda} = T \left(\frac{\partial s}{\partial T}\right)_{p_{ij},x_k',\lambda} \tag{133}$$

and satisfy equations of the form

$$C_{p_{11},x_2',\lambda} = C_{x_1',x_2',\lambda} - Tv_o \left(\frac{\partial p_{11}}{\partial T}\right)^2_{x_1',x_2',\lambda} \left(\frac{\partial x_1'}{\partial p_{11}}\right)_{T,x_2',\lambda} \tag{134}$$

$$C_{p_{11},x_1',\lambda} = C_{x_1',x_2',\lambda} - Tv_o \left(\frac{\partial p_{11}}{\partial T}\right)_{x_1',x_2',\lambda} \left(\frac{\partial p_{21}}{\partial T}\right)_{x_1',x_2',\lambda} \left(\frac{\partial x_2'}{\partial p_{11}}\right)_{T,x_1',\lambda} \tag{135}$$

The comparison of Equations (126) and (127) with Equations (130) and (131) demonstrates an important feature of shock-induced reactive flow. Because we expect the ratios of specific heats in Equations (130) and (131) to be approximately one and the derivatives $(\partial p_{11}/\partial \lambda)_{T,x_1',x_2'}$ and $(\partial p_{21}/\partial \lambda)_{T,x_1',x_2'}$ to be small compared to the derivatives $(\partial p_{11}/\partial \lambda)_{e,x_1',x_2'}$ and $(\partial p_{21}/\partial \lambda)_{e,x_1',x_2'}$, the temperature can increase along a particle path as the stresses decrease. Consequently, for a predominantly temperature dependent reaction rate, the rate of reaction can increase along a particle path as the stresses decrease, and the shock initiation of detonation can occur in a wave satisfying the condition $\partial p_{11}/\partial t < 0$.

We next consider the $e = e(T, v_o x_1', v_o x_2', \lambda)$ EOS and write its differential form as

$$de = C_{x_1', x_2', \lambda} dT + \left(\frac{\partial e}{\partial v_o x_1'}\right)_{T, x_2', \lambda} dv_o x_1' + \left(\frac{\partial e}{\partial v_o x_2'}\right)_{T, x_1', \lambda} dv_o x_2' + \left(\frac{\partial e}{\partial \lambda}\right)_{T, x_1', x_2'} d\lambda \tag{136}$$

To interpret the derivatives $(\partial e/\partial v_o x_1')_{T, x_2', \lambda}$ and $(\partial e/\partial v_o x_2')_{T, x_1', \lambda}$, we rewrite Equation (136) for a nonreactive fluid as

$$de = C_v dT + \left(\frac{\partial e}{\partial v_o x_1'}\right)_T dv \tag{137}$$

and use the first law of thermodynamics for adiabatic flow written as

$$de = - \delta W \tag{138}$$

to obtain the equation

$$C_v dT + \left(\frac{\partial e}{\partial v_o x_1'}\right)_T dv = - \delta W \tag{139}$$

We now recall that $(\partial e/\partial v_o x_1')_T$ is associated with forces of interaction among molecules and use Equation (139) to show that the work δW performed on a fluid is partitioned between thermal energy and repulsive energy when $(\partial e/\partial v_o x_1')_T < 0$. We also recall that for a gas with $(\partial e/\partial v_o x_1')_T = 0$, all the work is converted into thermal energy, but for a liquid with $(\partial e/\partial v_o x_1')_T < 0$, a large fraction of the work can be converted into the repulsive energy arising from compression. In Equation (136), we thus associate $(\partial e/\partial v_o x_1')_{T, x_2', \lambda}$ and $(\partial e/\partial v_o x_2')_{T, x_1', \lambda}$, respectively, with the repulsive forces arising from compression and, shear and on physical grounds, assume that $(\partial e/\partial v_o x_1')_{T, x_2', \lambda} / (\partial e/\partial v_o x_2')_{T, x_1', \lambda} \geq 1$.

We finally combine Equation (136) with Equation (39) to obtain the equation

$$C_{x_1', x_2', \lambda} \frac{\partial T}{\partial t} = - \left(\frac{\partial e}{\partial v_o x_1'}\right)_{x_2', \lambda, T} \frac{\partial v}{\partial t} - \left(\frac{\partial e}{\partial v_o x_2'}\right)_{x_1', \lambda, T} v_o \frac{\partial u_2}{\partial h_1} - \left(\frac{\partial e}{\partial \lambda}\right)_{T, x_1', x_2'} \frac{\partial \lambda}{\partial t}$$

$$- p_{11} \frac{\partial v}{\partial t} - p_{21} v_o \frac{\partial u_2}{\partial h_1} \tag{140}$$

3.3 MODEL REACTIVE SOLID FOR THE GAS GUN EXPERIMENTS

To include chemical reaction in our treatment of the PII experiment, we adopt the classical ZND model of detonation[14] and assume that the front of the wave produced in such an experiment is a nonreactive shock discontinuity. Because we are interested primarily in the dependence of the longitudinal particle velocity on the chemical reaction, it is convenient to restrict our attention to an equation of state for the reactive mixture that provides the most basic treatment of this dependence. Accordingly, we chose an equation of state that is compatible with the ideal inert flow discussed in Section 2.3 above. Properties that must be exhibited by this equation of state are derived as follows.

Conditions for the shear particle velocity in the reactive shock discontinuity at the wave front to remain zero can be inferred from the following equations, obtained respectively by setting $\partial\lambda/\partial t = 0$ in Equation (127) and differentiating Equation (47):

$$\frac{\partial p_{21}}{\partial t} = \left(\frac{\partial p_{21}}{\partial x_1'}\right)_{s,x_2'} \frac{\partial u_1}{\partial h_1} + \left(\frac{\partial p_{21}}{\partial x_2'}\right)_{s,x_1'} \frac{\partial u_2}{\partial h_1} \qquad (127)'$$

$$\frac{\partial p_{21}}{\partial t} = -\frac{dh_{1f}}{dt}\left(\frac{\partial p_{21}}{\partial h_1}\right)_{h_{1f}} - \rho_o \int_{h_{1f}}^{h_1} \left(\frac{\partial^2 u_2}{\partial t^2}\right) dh_1 \qquad (141)$$

It follows from Equations (127)' and (141) that the assumption that $\partial u_2/\partial t = 0$ in a leading inert isentropic CW is only truly valid for materials that satisfy the condition $(\partial p_{21}/\partial x_1')_{s,x_2'} = 0$. Now because $\partial u_2/\partial h_1 = 0$ when $\partial u_2/\partial t = 0$, it follows from Equation (97) written for the thermodynamic stresses that

$$\left(\frac{\partial p_{21}}{\partial x_1'}\right)_{s,x_2'} = \frac{\partial x_1}{\partial h_1}\frac{\partial t_{12}}{\partial V_{11}} \qquad (142)$$

We thus conclude that material subjected to PII will support a nonreactive CW with no shear velocity component when $\partial t_{12}/\partial V_{11}$ is proportional to V_{12}.

Conditions for the condition $\partial u_1/\partial t = 0$ to be satisfied in an ensuing, inert isentropic SW can be inferred from the following equations, obtained respectively by setting $\partial\lambda/\partial t = 0$ in Equation (126) and differentiating Equation (85):

$$\frac{\partial p_{11}}{\partial t} = \left(\frac{\partial p_{11}}{\partial x_1'}\right)_{s,x_2'} \frac{\partial u_1}{\partial h_1} + \left(\frac{\partial p_{11}}{\partial x_2'}\right)_{s,x_1'} \frac{\partial u_2}{\partial h_1} \tag{126}'$$

$$\frac{\partial p_{11}}{\partial t} = -\frac{dh_{1f}'}{dt}\left(\frac{\partial p_{11}}{\partial h_1}\right)_{h_{1f}'} - \rho_o \int_{h_{1f}'}^{h_1} \frac{\partial^2 u_1}{\partial t^2}\, dh_1 \tag{143}$$

It follows from Equations (126)' and (143) that the assumption that $\partial u_1/\partial t = 0$ in an ensuing inert isentropic SW is only truly valid for materials that satisfy the condition $(\partial p_{11}/\partial x_2')_{s,x_1'} = 0$. The equation

$$\left(\frac{\partial p_{11}}{\partial x_2'}\right)_{s,x_1'} = \frac{\partial x_1}{\partial h_1}\left(\frac{\partial x_2}{\partial h_1}\frac{\partial t_{11}}{\partial V_{11}} + \frac{\partial t_{11}}{\partial V_{12}}\right) \tag{144}$$

obtained by differentiating the equation relating p_{11} and t_{11} [Equation (33)], shows that the condition $(\partial p_{11}/\partial x_2')_{s,x_1'} = 0$ is much more restrictive than the condition $(\partial p_{21}/\partial x_1')_{s,x_2'} = 0$.

It follows from the above discussion that the ideal inert flow described in Section 2.3 can be modeled by using an EOS satisfying the following conditions:

$$\left(\frac{\partial^2 p_{11}}{\partial (x_1')^2}\right)_{s,x_2',\lambda} = \left(\frac{\partial p_{11}}{\partial x_2'}\right)_{s,x_1',\lambda} = \left(\frac{\partial p_{21}}{\partial x_1'}\right)_{s,x_2',\lambda} = 0 \tag{145}$$

A simple model EOS that has the initial hydrostatic stress $p_o = 0$ and satisfies these conditions is conveniently written in terms of x_2' and the displacement gradient, $u' = \partial u/\partial h_1 = x_1' - 1$, as follows:

$$e = e_o^x - \lambda Q + \frac{v_o}{2} A_1(s)(u')^2 + \frac{v_o}{2} A_2(s)(x_2')^2 \tag{146}$$

It follows from the definition of u' that we can set $(\partial/\partial u') = (\partial/\partial x_1')$ when we differentiate Equation (146). Differentiating Equation (146) partially with respect to λ, s, u', and x_2' leads to the following equations for A, T, p_{11}, and p_{21}:

$$A = Q \tag{147}$$

$$T = \frac{v_o}{2}\left[(u')^2 \frac{dA_1}{ds} + (x')^2 \frac{dA_2}{ds}\right] \tag{148}$$

$$-p_{11} = A_2(s)u' \tag{149}$$

$$-p_{21} = A_2(s)x_2' \tag{150}$$

It is clear from these equations that we are neglecting the difference between A and Q, the initial temperature, and the derivatives $(\partial p_{21}/\partial\lambda)_{s,x_1',x_2'}$ and $(\partial p_{21}/\partial\lambda)_{s,x_1',x_2'}$. Some Maxwell relationships that we will use later are obtained by differentiating Equations (148), (149), and (150) as

$$\left(\frac{\partial T}{\partial v_o x_1'}\right)_{s,x_2',\lambda} = u' \frac{dA_1}{ds} = -\left(\frac{\partial p_{11}}{\partial s}\right)_{x_1',x_2',\lambda} \tag{151}$$

$$\left(\frac{\partial T}{\partial v_o x_2'}\right)_{s,x_1',\lambda} = x_2' \frac{dA_2}{ds} = -\left(\frac{\partial p_{21}}{\partial s}\right)_{x_1',x_2',\lambda} \tag{152}$$

It is also clear from Equations (149) and (150) that our model EOS satisfies the last two conditions expressed in equation (145). For consistency with the theory of elasticity, we set $A_1(s) = \delta + 2\mu$, $A_2(s) = \mu$ and note that δ is used in the expression for $A_1(s)$ because λ has already been used for the reaction coordinate. Equations (149) and (150) then give the following governing equations for our ideal inert flow in a PII experiment:

$$p_{11} = -(\delta + 2\mu)u' \tag{153}$$

$$p_{21} = - \mu x_2' \tag{154}$$

$$\left(\frac{\partial p_{11}}{\partial x_1'}\right)_{s,x_2',\lambda} = - A_1(s) = - (\delta + 2\mu) \tag{155}$$

$$\left(\frac{\partial p_{21}}{\partial x_2'}\right)_{s,x_1',\lambda} = - A_2(s) = - \mu \tag{156}$$

$$\left(\frac{\partial^2 p_{11}}{\partial (x_1')^2}\right)_{s,x_2',\lambda} = \left(\frac{\partial^2 p_{21}}{\partial (x_2')^2}\right)_{s,x_1',\lambda} = 0 \tag{157}$$

After combining Equations (73), (74), (155), and (157) and Equations (105), (106), (156), and (157), we conclude that in the absence of a chemical reaction, the isentropic discontinuity at the front of the pure CW propagates at the velocity $C_1 = [v_o(\delta + 2\mu)]^{1/2}$, and the isentropic discontinuity at the front of the ensuing pure SW propagates at the velocity $C_2 = (v_o\mu)^{1/2}$.

We are now in a position to consider our model for the reactive flow produced in a PII experiment. The combination of the time derivative of equation (146) with the first law of thermodynamics expressed by Equation (39) leads to the following equation for the entropy production

$$T \frac{\partial s}{\partial t} = Q \frac{\partial \lambda}{\partial t} \tag{158}$$

which shows that the only irreversible process being considered is the chemical reaction. The other equations governing our reactive flow can readily be derived as follows.

We combine the equations obtained by differentiating Equations (149) and (150) with Equations (148) and (158) to obtain the time derivatives of p_{11} and p_{21} as

$$\frac{\partial p_{11}}{\partial t} = \left(\frac{\partial p_{11}}{\partial x_1'}\right)_{s,x_2',\lambda} \frac{\partial u_1}{\partial h_1} - \frac{2u'(dA_1/ds)\ Q}{v_o\left[(u')^2 dA_1/ds + (x_2')^2 dA_2/ds\right]} \frac{\partial \lambda}{\partial t} \tag{159}$$

$$\frac{\partial p_{21}}{\partial t} = \left(\frac{\partial p_{21}}{\partial x_2'}\right)_{s,x_1',\lambda} \frac{\partial u_2}{\partial h_1} - \frac{2x_2'(dA_2/ds)Q}{v_o\left[(u')^2 dA_1/ds + (x_2')^2 dA_2/ds\right]} \frac{\partial \lambda}{\partial t} \qquad (160)$$

It then follows from Equations (126) and (127) that for our EOS

$$\left(\frac{\partial p_{11}}{\partial \lambda}\right)_{e,x_1',x_2'} = - \frac{2u'(dA_1/ds)Q}{v_o\left[(u')^2 dA_1/ds + (x_2')^2 dA_2/ds\right]} \qquad (161)$$

$$\left(\frac{\partial p_{21}}{\partial \lambda}\right)_{e,x_1',x_2'} = - \frac{2x_2'(dA_2/ds)Q}{v_o\left[(u')^2 dA_1/ds + (x_2')^2 dA_2/ds\right]} \qquad (162)$$

To obtain the equation relating the time derivatives of the stresses, we add the equations obtained by multiplying Equation (159) by u' and Equation (160) by x'.

$$- \left(u' \frac{\partial p_{11}}{\partial t} + x_2' \frac{\partial p_{21}}{\partial t}\right) = - p_{11} \frac{\partial u_1}{\partial h_1} - p_{21} \frac{\partial u_2}{\partial h_1} + \frac{2Q}{v_o} \frac{\partial \lambda}{\partial t} \qquad (163)$$

It is clear that Equation (163) can also be derived by combining the time derivative of Equation (146) written as

$$e = e_o^x - \lambda Q - \frac{v_o}{2} p_{11} u' - \frac{v_o}{2} p_{21} x_2' \qquad (164)$$

with the first law of thermodynamics expressed by Equation (39).

Equations (159) through (163) provide us with a convenient basis for understanding the results of our gas gun experiments. The equations governing reactive compressive flow produced by normal impact are obtained as

$$\frac{\partial p_{11}}{\partial t} = \left(\frac{\partial p_{11}}{\partial x_1'}\right)_{s,x_2',\lambda} \frac{\partial u_1}{\partial h_1} - \frac{2Q}{v_o u'} \frac{\partial \lambda}{\partial t} \qquad (165)$$

$$\frac{\partial p_{21}}{\partial t} = 0 \qquad (166)$$

by setting $x_2' = \partial u_2/\partial h_1 = 0$ in Equations (159), (160), and (163). It then follows that reactive flow produced by PII is governed by Equations (165) and (166) in regions where $x_2' = \partial u_2/\partial h_1 = 0$ and by Equations (159) through (163) in regions where $x_2' \neq 0$. We thus expect the sets of longitudinal particle velocity histories recorded in equivalent normal-impact and PII experiments to exhibit essentially the same flow features until reaction occurs in regions influenced by shear deformation.

Further consideration of these reactive flow equations leads us to conclude that the flows produced by normal-impact and PII depend on the relative time scales for CIR, SIR, shear wave propagation, and the one-dimensional flow in our experiments.

Three types of flow determined by the relative magnitudes of these time scales are postulated to provide a means of interpreting the results of our gas gun experiments. We label these flows as types I, II, and III and characterize them as follows:

- In type I flow, the one-dimensional time of our gas gun experiment is shorter than the time scales for CIR and SIR.
- In type II flow, the one-dimensional time of our gas gun experiment is shorter than the time scale for CIR but longer than that for SIR.
- In type III flow, the one-dimensional time of our gas gun experiment is longer than the time scale for CIR.

In the next two subsections, we will consider the occurrence of these types of flows in a series of gas gun experiments performed with increasing flyer velocities to provide a framework for interpreting the sets of longitudinal particle velocity histories we have recorded in Composition B3.

3.3.1 Flows Influenced by Compression-Induced Reaction

We now present a more detailed account of the influence of CIR on the shock-induced flow produced by normal-impact and PII. Because reaction at the shock front influences the values of the longitudinal particle velocity (u_1) and the compressional stress $(p_{11})_H$ there, we

first write the equations for the time rate of change of these quantities as

$$\frac{d(u_1)_H}{dt} = \frac{\partial u_1}{\partial t}_H + C_1\left(\frac{\partial u_1}{\partial h_1}\right)_H \tag{167}$$

$$\frac{d(p_{11})_H}{dt} = \frac{\partial p_{11}}{\partial t}_H + C_1\left(\frac{\partial p_{11}}{\partial h_1}\right)_H \tag{168}$$

It follows from Equations (167) and (168) that $(u_1)_H$ and $(p_{11})_H$ will remain unchanged as the CW propagates if either $(\partial u_1/\partial t)_H = (\partial u_1/\partial h_1)_H = 0$ and $(\partial p_{11}/\partial t)_H = (\partial p_{11}/\partial h_1)_H = 0$ or $(\partial u_1/\partial t)_H = - C_1(\partial u_1/\partial h_1)_H$ and $(\partial p_{11}/\partial t)_H = - C_1(\partial p_{11}/\partial h_1)_H$.

Because shock-induced reactive flow is complicated, we will now concentrate largely on a type of compressive flow that we have observed in our present investigation of Composition B3. In this type of flow, which has also been observed in multiple Lagrange gage studies of other explosives such as TNT[15] and PBX9404,[16] the shock propagates essentially unchanged until it is overtaken by a reactive stress wave from the rear. We are consequently interested in shock-induced flows with $\partial p_{11}/\partial t > 0$, $\partial p_{11}/\partial h_1 < 0$, and $\partial u_1/\partial t > 0$. Although such flows can develop initially with either $\partial u_1/\partial h_1 < 0$ or $\partial u_1/\partial h_1 > 0$, we will only consider the latter case here.

It is convenient to use the following equations

$$\frac{\partial p_{11}}{\partial t} = \left(\frac{\partial p_{11}}{\partial x_1'}\right)_{s,x_2',\lambda} \frac{\partial u_1}{\partial h_1} + \left(\frac{\partial p_{11}}{\partial \lambda}\right)_{e,x_1',x_2'} \frac{\partial \lambda}{\partial t} \tag{159}'$$

$$\frac{\partial p_{11}}{\partial h_1} = \left(\frac{\partial p_{11}}{\partial h_1}\right)_H + \int_{\tau_1}^{t} \frac{\partial^2 p_{11}}{\partial t \partial h_1}\, dt \tag{169}$$

$$\frac{\partial p_{21}}{\partial t} = \left(\frac{\partial p_{21}}{\partial x_2'}\right)_{s,x_1',\lambda} \frac{\partial u_2}{\partial h_1} + \left(\frac{\partial p_{21}}{\partial \lambda}\right)_{e,x_1',x_2'} \frac{\partial \lambda}{\partial t} \tag{160}'$$

in our discussion of a series of gas gun experiments performed with increasing flyer velocities. To provide a better appreciation of flow influenced by CIR, we first chose the lower flyer velocities in normal-impact and PII experiments to produce flows of type I. In this case, flows are nonreactive in the time frame of the experiments and the CWs propagate as step shocks with $\partial u_1/\partial t = \partial u_1/\partial h_1 = 0$.

We thus expect the sets of longitudinal particle velocity histories produced at the lower flyer velocities in our gas gun experiments to exhibit the same features.

As the flyer velocities are increased, the shock becomes strong enough to initiate CIR in the time frame of the experiment and we must consider flows of type III. Remembering that we are primarily interested in type III flow with the energy release rate essentially zero at the shock front and $\partial u_1/\partial h_1 \geq 0$, we first consider the flows in the CWs where $x_2' = \partial u_2/\partial h_1 = \partial p_{21}/\partial t = 0$. Because $\partial u_1/\partial h_1 = 0$ initially, it follows from Equation (159)' that the stress increases along a particle path, $\partial p_{11}/\partial t > 0$, as the reaction rate increases. Thereafter, because $\partial u_1/\partial h_1 > 0$, the stress continues to increase along a particle until it attains a maximum, $\partial p_{11}/\partial t = 0$, at the time when the chemical energy release rate term is balanced by the particle velocity gradient term. Thereafter, the stress falls along a particle path until the chemical energy release rate becomes zero and the flow becomes isentropic. We next use Equation (169) to determine conditions for u_1 to increase along a particle path as p_{11} increases. Because $(\partial p_{11}/\partial h_1)_H \simeq 0$, it follows from the momentum equation and Equation (169) that u_1 will increase with p_{11} along a particle path when $\partial^2 p_{11}/\partial t \partial h_1 < 0$. We thus expect u_1 to increase along a particle path when the energy release rate on the particle path immediately to its left is greater than the energy release rate on the particle path immediately to its right.

Having considered the compressive reactive flow produced in equivalent normal-impact and PII experiments, we must now consider the additional influence of CIR on the flow produced by PII. Now because $(\partial p_{21}/\partial \lambda)_{e,x_1',x_2'} \neq 0$ when $x_2' \neq 0$, CIR influences material subjected to

shear deformation, and it follows from Equations (160)' and (163) that the energy released by chemical reaction influences both $\partial p_{21}/\partial t$ and $\partial p_{11}/\partial t$ and is consequently converted into the shear particle velocity field as well as the longitudinal particle velocity field. In type III flows influenced by CIR, we thus expect more chemical energy to be converted into the longitudinal particle velocity field in normal-impact experiments than in PII experiments.

For the reasons given in this discussion, we expect the sets of longitudinal particle velocity histories recorded in equivalent normal-impact and PII experiments to exhibit the same type III flow features until the material subjected to shear strain in the PII experiment is influenced by chemical reaction. In the absence of SIR, differences between these sets of records occur because chemical energy is partitioned between the longitudinal and shear particle velocity fields in the PII experiment but not in the normal-impact experiment. We thus conclude that qualitative differences between sets of longitudinal particle velocity histories recorded in equivalent normal-impact and PII experiments that exhibit type III flow cannot be taken as evidence for the occurrence of SIR.

The influence of SIR on type III flows will be discussed in the next subsection.

We finally note that type III flows exhibiting different features will be produced as the flyer velocity is increased, because the shock becomes significantly influenced by the energy release rate at the shock front.

3.3.2 Flows Influenced by Shear-Induced Reaction

From our classification of flows produced in our gas gun experiments, it is clear that SIR will first occur in flows of type II produced by fliers with velocities too low to initiate CIR. We thus consider flows exhibiting a nonreactive CW, $(\partial p_{11}/\partial \lambda)_{e,x_1',x_2'}$, $\partial \lambda/\partial t = 0$, and chemical reaction initiated by the shear deformation resulting from PII. In this

follows from Equations (160)' and (162) that the shear stress starts to increase along a particle path, $\partial p_{21}/\partial t > 0$. Moreover, because $\partial u_1/\partial h_1$ is initially zero but $u' \neq 0$ in the region where $x_2' \neq 0$, it follows from Equations (159)' and (161) that the normal stress p_{11} also starts to increase along a particle path, $\partial p_{11}/\partial t > 0$. These changes in p_{21} and p_{11}, produced along a particle path by the energy liberated by SIR, are related by Equation (163). It then follows that the stress gradients $\partial p_{11}/\partial h_1$ and $\partial p_{21}/\partial h_1$, resulting from the spatial variations of $\partial p_{11}/\partial t$ and $\partial p_{21}/\partial t$, will produce corresponding changes in u_1 and u_2 governed by the momentum equations. We thus expect the sets of longitudinal particle velocity histories recorded in such equivalent normal-impact and PII experiments to exhibit the same features until the flow produced by PII is influenced by SIR. We believe that we have just formulated a more precise but qualitative account of Gupta's approach[3] to the problem of SIR in explosives.

We now return to type III flows produced in normal-impact and PII experiments and consider the case when the reaction rate is enhanced by the shear deformation. It follows from our discussion of Equation (136) that such enhancement is possible in our reactive solid when the reaction rate is primarily temperature dependent, because most of the shear work is converted into temperature. It also follows from our previous discussion in this section that the additional chemical energy released in the PII experiment will influence both the longitudinal and shear particle velocity histories. Thus, we again expect the sets of longitudinal particle velocity histories exhibiting type III flow to differ, because chemical energy is partitioned between the longitudinal and shear particle velocity fields in the PII experiment but not in the normal impact experiment.

We thus conclude that evidence for SIR cannot readily be obtained by comparing sets of longitudinal particle velocity histories from normal-impact and PII experiments that exhibit type III flow, because differences between these sets of histories can be attributed to the influence of either CIR or SIR on the flow produced by PII.

4. EXPERIMENTAL METHODS AND RESULTS

This section describes the methods used to prepare the Composition B3 targets and the results of the normal and parallel-inclined impact experiments.

4.1 MULTIPLE LAGRANGE GAGE COMPOSITION B3 TARGETS

Targets of Composition B3 (60% RDX, 40% TNT by weight) were used in all the gas gun experiments. These targets were made as pucks by casting Composition B3 around sets of Lagrange particle velocity gages held in a gage assembly. The casting was performed at SRI International's Test Facility, and preliminary castings were sectioned to verify that the casting procedure produced uniform Composition B3 with no cavities and with the gages firmly embedded in the explosive. The gage assemblies used for casting four cylindrical targets 40 mm in diameter and 20 mm high, each containing three Lagrange gages, were made at SRI. Figure 4-1 is a photograph of a gage assembly showing three particle velocity gages before casting. These gages were positioned 0.5, 2.5, and 4.5 mm above the base plate of the assembly, which interfaces with the impact surface of the explosive target. The 10-mm-long active gage elements were made from 0.05-mm-diameter copper wires and carefully soldered to 0.25-mm-diameter copper posts. After the casting process, the copper posts came out of the back surface of the explosive target, as indicated in Figure 4-1. The explosive targets were backed with 6-8 mm of epoxy before they were potted in the Lucite target ring required for the gas gun experiment.

4.2 GAS GUN EXPERIMENTS

We performed eighteen gas gun experiments with five batches of Composition B3. These shots were peformed in sets and were labelled in chronological order as follows: (84-2-26, 84-2-27, 84-2-28), (84-2-33,

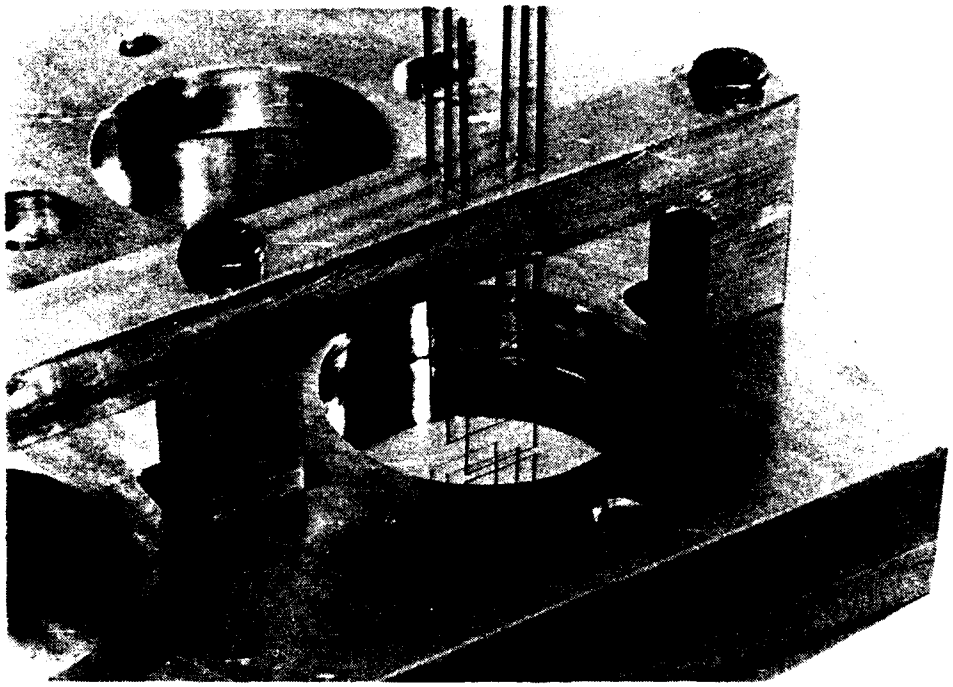

RP-6834-1

Figure 4-1. Photograph of gage assembly showing three particle velocity gages before the casting process.

84-2-34, 84-2-35, 84-2-36), (85-2-8, 85-2-9, 85-2-10, 85-2-11), (86-2-16, 86-2-17, 86-2-18), and (86-2-64, 86-2-65, 86-2-66, 86-2-67). The results of these experiments are summarized in Table 4-1.

We will discuss these sets of experiments in chronological order but will not present all the particle velocity histories because some experiments are repeats of others and because some of the particle velocity histories are too noisy to be useful.

4.2.1 The First Set of Shots

The first set of experiments was designed to produce an initial compressional stress in Composition B3 in the 20-kbar region. The magnetic field was oriented to measure the longitudinal particle velocity histories produced by normal impact in Shot 84-2-26 and by PII (15° angle) in Shot 84-2-28 and the shear particle velocity histories produced by PII (15° angle) in Shot 84-2-27. Figure 4-2(a) shows a composite plot of the longitudinal particle velocity histories produced in Shot 84-2-26 by the normal impact of a 1/4-inch-thick fused silica flyer travelling at 0.558 mm/μs, and Figure 4-2(b) shows a composite plot of those produced in Shot 84-2-28 by the PII of a 3/8-inch-thick fused silica flyer travelling at 0.575 mm/μs. When interpreting these particle velocity histories, it is important to remember that the experimental frame time at a gage location is ~3.5 μs. Data beyond 3.5 μs are questionable because of lead effects.

We now recall that our investigation of SIR is based on a comparison of the sets of longitudinal particle velocity histories produced by similar compressional loading conditions in normal-impact and PII experiments. Sets of histories were compared by superpositioning one set of histories on the other. Superposition of the histories in Figures 4-2(a) and 4-2(b) showed (1) that these sets of histories cannot be compared at all three gage positions because the CW broke the third gage in the normal-impact experiment, and (2) that the histories recorded by the first and second gages in both types of impact experiment are essentially the same when the flyer plate thicknesses are taken into account. Comparison of the histories in Figure 4-2(b) reveals

Table 4-1

SUMMARY OF COMPRESSION-SHEAR EXPERIMENTS
PERFORMED IN COMPOSITION B3[a]

Shot No.	Flyer Velocity (mm/μs)	Angle Degrees	Initial Particle Velocity (mm/μs)	Comments
84-2-26[b]	0.558	0°	0.416	Third gage broke
84-2-27[c]	0.579	15°	None	No good records
84-2-28[b]	0.575	15°	0.414	Reactive flow
84-2-33[b]	0.295	0°	0.215	Reactive flow
84-2-34[b]	0.292	15°	0.220	Reactive flow
84-2-35[c]	0.302	15°	None	No good records
84-2-36[b]	0.300	15°	None	First gage record too noisy
85-2-8[b]	0.301	0°	0.216	Reactive flow
85-2-9[b]	0.305	15°	0.200	Reactive flow
85-2-10[b]	0.308	20°	0.200	Reactive flow
85-2-11[c]	0.312	15°	None	No good records
86-2-16[b]	0.294	0°	None	First gage record too noisy
86-2-17[b]	0.304	15°	0.140	Essentially nonreactive
86-2-18[b]	0.294	15°	0.136	Second gage faulty
86-2-64[b]	0.293	0°	0.230	Essentially nonreactive
86-2-65[b]	0.302	15°	0.230	Essentially nonreactive
86-2-66[b]	0.452	15°	0.310	Reactive flow
86-2-67[b]	0.429	0°	0.320	Reactive flow

[a]A 1/4-inch-thick fused silica flyer was used in Shot 84-2-26; 3/8-inch-thick fused silica flyers were used in all the others.

[b]Magnetic field aligned to measure longitudinal particle velocity.

[c]Magnetic field aligned to measure shear particle velocity.

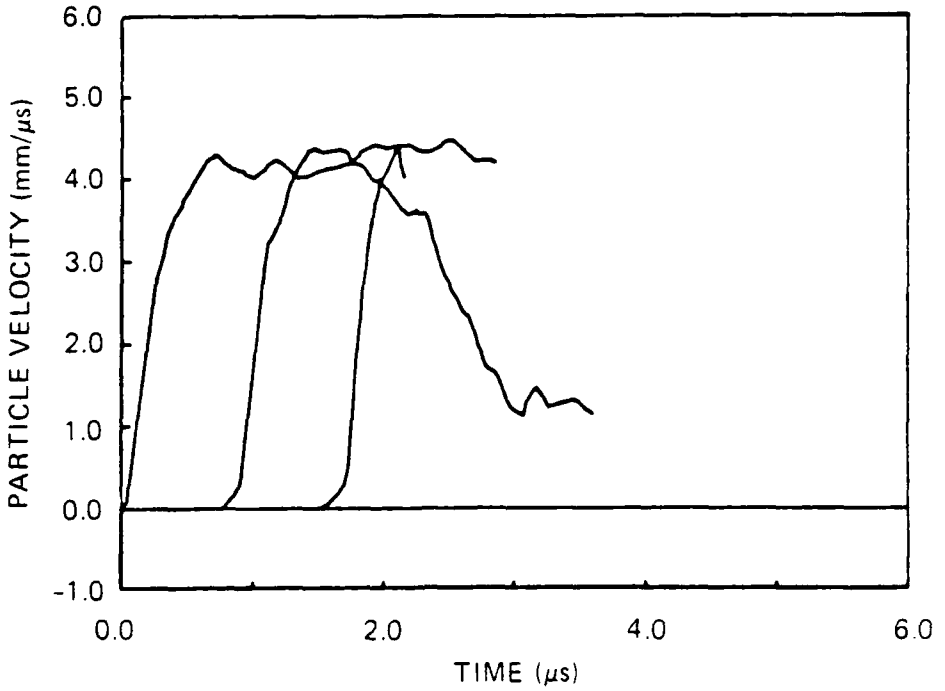

(a) Shot 84-2-26, normal impact

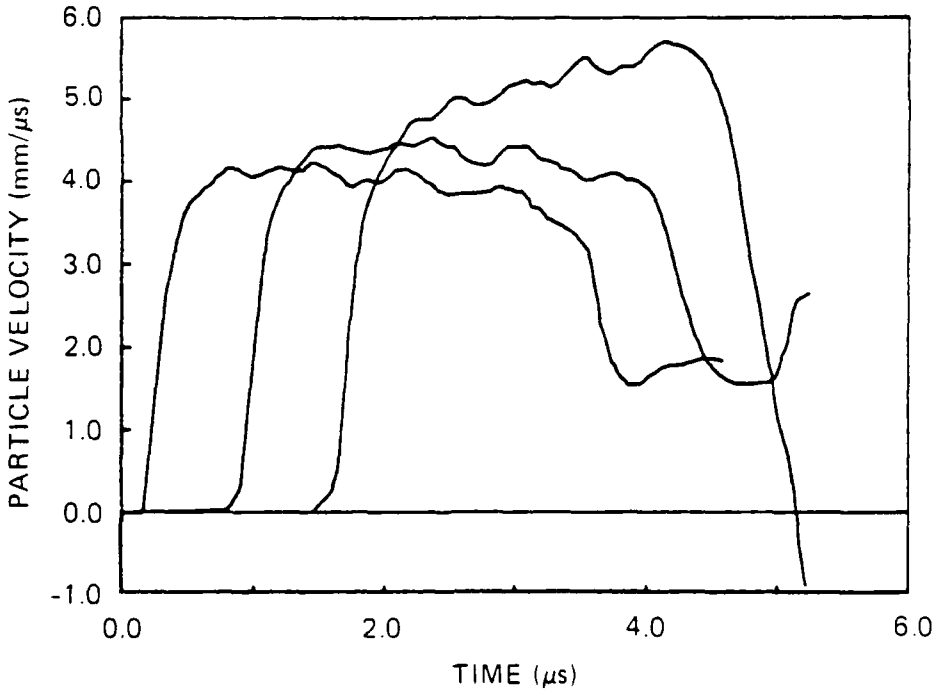

(b) Shot 84-2-28, parallel-inclined impact (15° angle)

JA-6834-1

Figure 4-2. Composite plots of Lagrange longitudinal particle velocity histories in Composition B3 produced by normal impact in Shot 84-2-26 and by parallel-inclined impact (15° angle) in Shot 84-2-28.

developing flow features characteristic of a type III flow, produced by a shock strong enough to initiate a significant energy release rate at the shock front. The particle velocity $(u_1)_H$ at the shock front increases $d(u_1)_H/dt > 0$, and until the flow behind the shock is influenced by the rarefaction from the rear of the flyer plate, the compressional stress gradient, $\partial p_{11}/\partial h_1$, is zero at the first and second gage positions, where $\partial u_1/\partial t = 0$, but is negative at the third gage position where $\partial u_1/\partial t > 0$. Because $d(u_1)_H/dt > 0$, it follows from Equation (166) that the energy release rate at the shock front is sufficient to make $d(p_{11})_H/dt > 0$ and $(\partial p_{11}/\partial t)_H > 0$. In addition, the energy released by CIR behind the shock front causes p_{11} to increase along a particle path in such a way that the second derivative $(\partial^2 p_{11}/\partial t \partial h_1)$ is zero in the neighborhood of the first two gages but negative in the neighborhood of the third gage.

We conclude from this discussion that our first set of shots is inconclusive with regard to SIR because the initial compressional loading in the 20-kbar region produces a type III flow that is significantly influenced by CIR.

The records from Shot 84-2-27, the experiment designed to produce shear particle velocity histories, are not presented because no significant shear particle velocity was recorded beyond the first gage position.

4.2.2 The Second Set of Shots

The second set of experiments was designed to produce an initial compressional stress in Composition B3 in the 10-kbar region. The magnetic field was oriented to measure the longitudinal particle velocity histories produced by normal impact in Shot 84-2-33 and by PII (15° angle) in Shots 84-2-34 and 84-2-36 and the shear particle velocity histories produced by PII (15° angle) in Shot 84-2-35. Shot 84-2-36 was performed as a repeat of Shot 84-2-34 to test the reproducibility of our experimental technique, but the excessive noise recorded at some of its gage positions invalidated this test. This is also the reason why we do not present the records from Shot 84-2-36.

A 3/8-inch-thick fused silica flyer was used in all of these shots. Figure 4-3(a) shows a composite plot of the longitudinal particle velocity histories produced in Shot 84-2-33 by the normal-impact of a flyer travelling at 0.295 mm/μs, and Figure 4-3(b) shows a composite plot of those produced in Shot 84-2-34 by the PII (15° angle) of a flyer travelling at 0.292 mm/μs. The voltage traces recorded in Shot 84-2-34 by the analog oscilloscopes are also presented (Figure 4-4) to exemplify the quality of the particle velocity data usually recorded in our experiments.

Superposition of the histories in Figures 4-3(a) and 4-3(b) shows (1) that the sets of histories can be compared at all three gage positions, and (2) that the flows recorded in Shots 84-2-33 and 84-2-34 initially developed in the same way but then became significantly different. Properties of the particle velocity histories recorded in both shots are discussed in some detail below to specify the similarities and differences between the two flows.

Qualitatively, the particle velocity histories recorded at the first gage plane are similar and exhibit, behind the wave front, a region of constant particle velocity followed by a region where the particle velocity rises to a peak and then falls. Quantitatively, these histories are essentially identical for 1.76 μs and then become different. After 1.76 μs, the particle velocity recorded in Shot 84-2-34 rises to peak value of 0.275 mm/μs at 3.0 μs, but the particle velocity recorded in Shot 84-2-33 remains essentially constant for another 0.5 μs before rising to a peak value of 0.239 mm/μs at 2.78 μs.

Qualitatively, the particle velocity histories recorded at the second gage plane are different in the sense that the history from Shot 84-2-34 exhibits a well-defined particle velocity peak but the history from Shot 84-2-33 does not. Quantitatively, however, these histories are essentially identical for 1.06 μs. After 1.06 μs, the particle velocity recorded in Shot 84-2-34 rises to a peak value of 0.219 mm/μs at 2.12 μs, but the particle velocity recorded in Shot 84-2-33 remains essentially constant for most of the history.

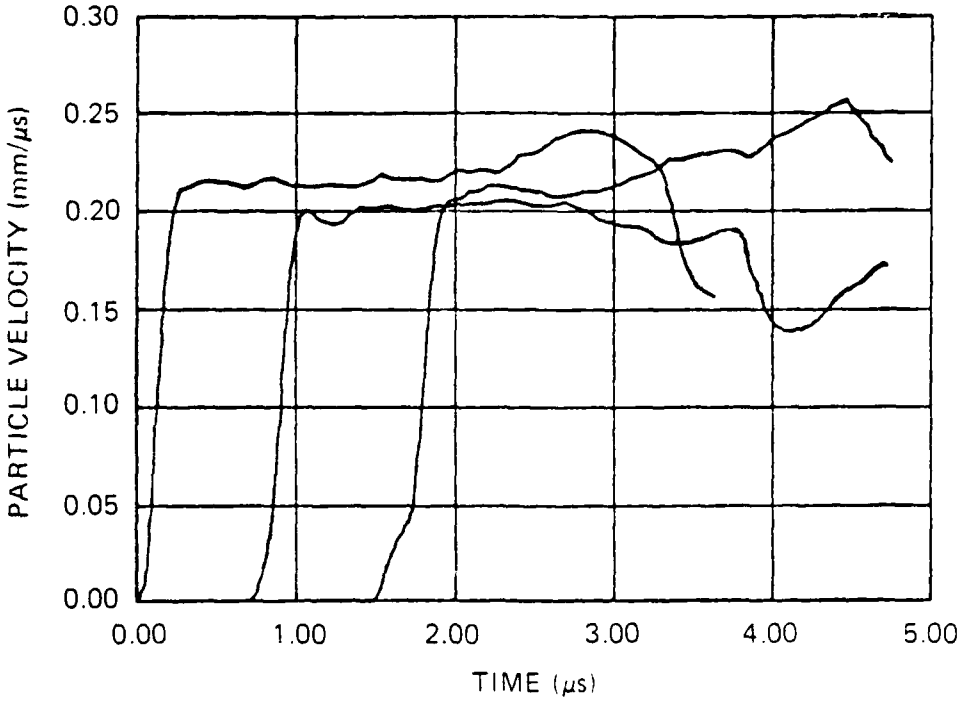

(a) Shot 84-2-33, normal impact

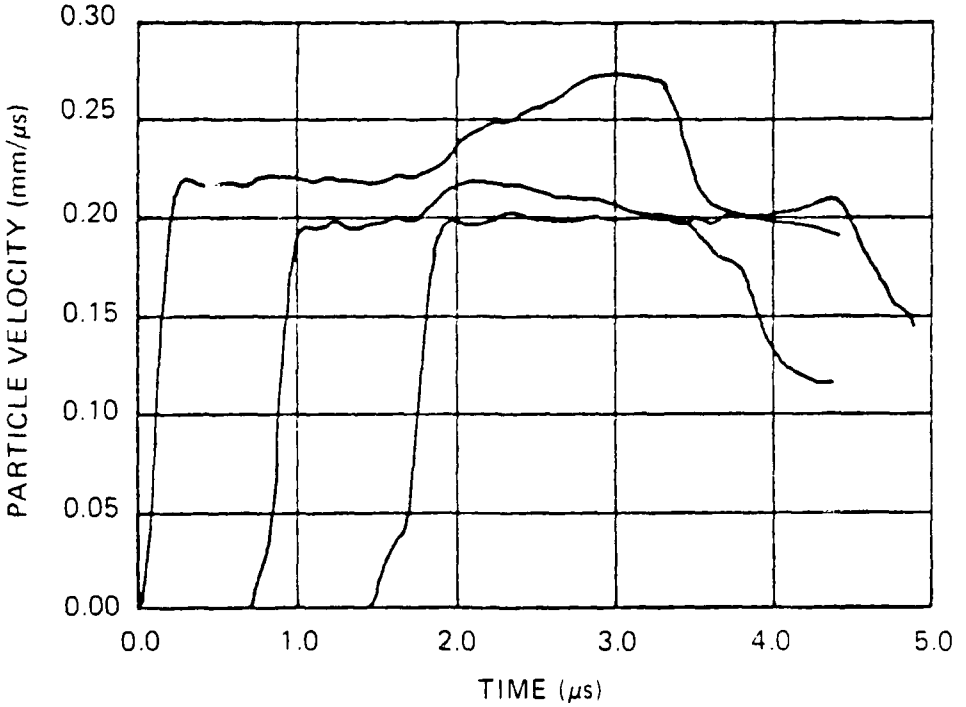

(b) Shot 84-2-34, parallel-inclined impact (15° angle)

JA-6804-2

Figure 4-3. Composite plots of Lagrange longitudinal particle velocity histories in Composition B3 produced by normal impact in shot 84-2-33 and by parallel-inclined impact (15° angle) in Shot 84-2-34.

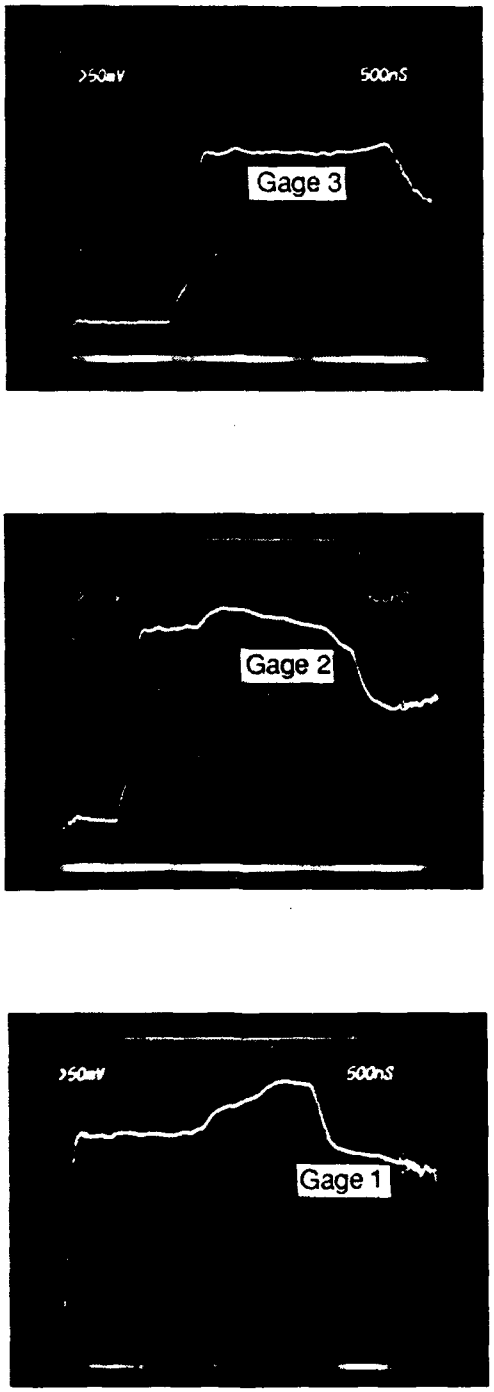

RP-6834-2

Figure 4-4. Electromagnetic particle velocity gage records from the analog oscilloscopes in Shot 84-2-34.

The particle velocity histories recorded at the third gage plane are both qualitatively and quantitatively different. The particle velocity in Shot 84-2-34 rises to a value of 0.2 mm/μs at the wave front and remains constant for 2 μs. However, the particle velocity recorded in Shot 84-2-33 rises to a value of 0.207 mm/μs at the wave front, continues to rise and attains a value of 0.213 mm/μs at 2.25 μs, then falls to a value of 0.207 mm/μs at 2.68 μs, and finally rises to a value of 0.25 mm/μs at 4.33 μs.

Further examination of these sets of particle velocity histories leads us to consider two alternative interpretations of these flows. In the first interpretation, we take the records at face value and see that both flows develop as the same decaying step shock in the $(p_{11} - h_1)$ plane until the particle velocity starts to increase in the PII experiment. Therefore, the stress gradient becomes negative at the first and second gage planes in Shot 84-2-34 and at the first gage plane in Shot 84-2-33. We now use Equation (168) to show that $(\partial p_{11}/\partial t)_H < 0$ at the front of the decaying shock because $d(p_{11})_H/dt < 0$ and $(\partial p_{11}/\partial h_1)_H = 0$, and to infer that $\partial p_{11}/\partial t < 0$ and $\partial^2 p_{11}/\partial t \partial h_1 = 0$ in the decaying step shock where $\partial u_1/\partial t = 0$.

We can then, by extending our previous discussions of reactive flow, associate the decaying step shock with a negative, global, energy release rate and the ensuing negative stress gradients with a positive, global, energy release rate. This being the case, it is important to note (1) that the negative stress gradient appears first in the flow produced by PII in Shot 84-2-34, and (2) that the particle velocity in Shot 84-2-34 increases for a longer period of time and attains a significantly higher peak value than that in Shot 84-2-33.

In the second interpretation of these two flows, the differences between the shock particle velocities $(u_1)_H$ recorded at the first and second gage planes in both shots are neglected for practical purposes. Then the global energy release rate in both flows is considered to be initially zero, but our previous argument associating the negative stress gradients with a positive energy release rate is still valid.

From these two interpretations of the flows recorded in Shots 84-2-33 and 84-2-34, we conclude that the influence of the energy release rate occurs first in the flow produced by PII, and consequently, we designate this flow as a kind of type II flow. We then accordingly attribute the significant differences between the sets of longitudinal particle velocity histories recorded in Shots 84-2-33 and 84-2-34 to the occurrence of SIR.

The records from Shot 84-2-35 are not presented because they are too noisy.

4.2.3 The Third Set of Shots

The third set of experiments was also designed to produce an initial compressional stress in Composition B3 in the 10-kbar region. The magnetic field was oriented to measure the longitudinal particle velocity histories produced by normal impact in Shot 85-2-8, by PII (15° angle) in Shot 85-2-9, and by PII (20° angle) in Shot 85-2-10; and the shear particle velocity histories produced by PII (15° angle) in Shot 85-2-11. A 3/8-inch-thick fused silica flyer was used in all of these experiments. Composite plots of the longitudinal particle velocities recorded in Shot 85-2-8 (0° angle) with the flyer travelling at 0.301 mm/μs; in Shot 85-2-9 (15° angle), with the flyer travelling at 0.305 mm/μs; and in Shot 85-2-10 (20° angle), with the flyer travelling at 0.308 mm/μs; are shown in Figures 4-5 through 4-7. The results of the shear particle velocity measurements obtained in Shot 85-2-11 (15° angle), with the flyer travelling at 0.312 mm/μs, are shown in Figure 4-8. These records from Shot 85-2-11 are presented here to typify the results of our shear particle velocity measurements in this work and demonstrate our inability to record well-defined shear particle velocity histories in Composition B3.

Superposition of the sets of longitudinal particle velocity histories in Figures 4-5 through 4-7 leads to three important observations. The first is that the flows produced by normal-impact and PII in Shots 85-2-8, 85-2-9, and 85-2-10 are for practical purposes the same until they are significantly influenced by the energy release rate. The second

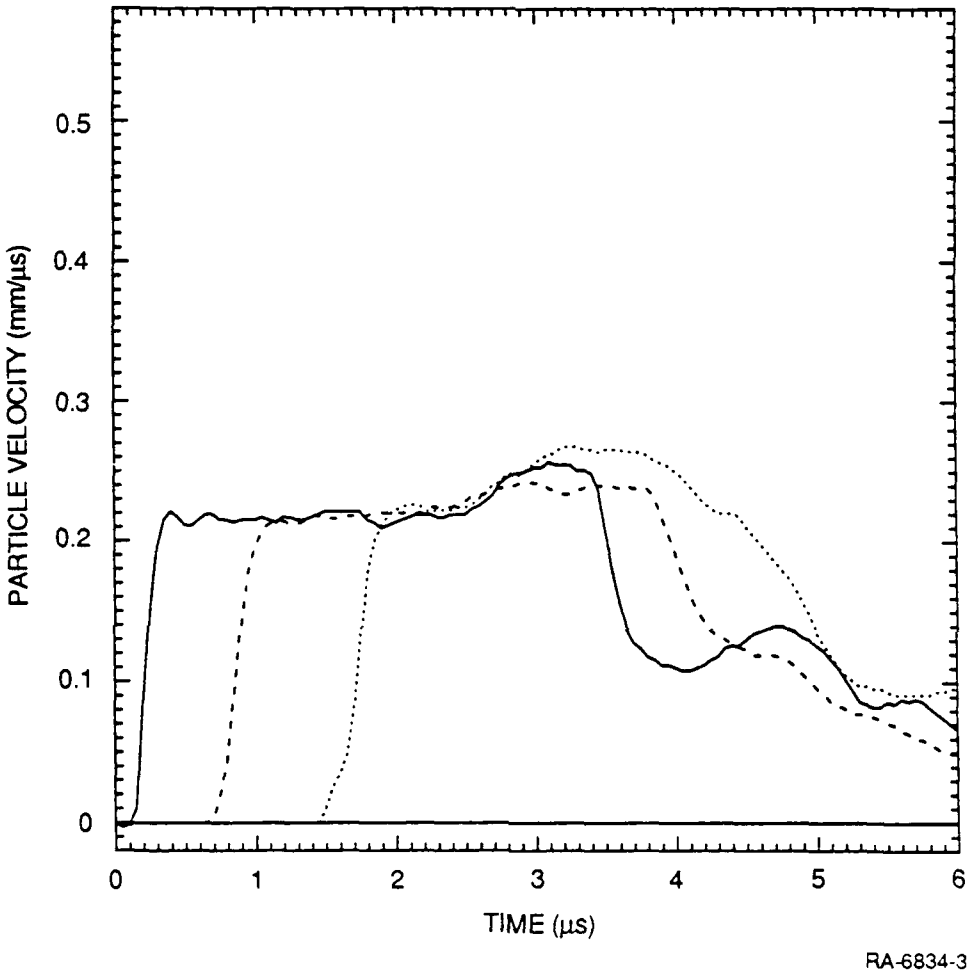

Figure 4-5. Composite plot of Lagrange longitudinal particle velocity histories in Composition B3 produced by normal impact in Shot 85-2-8.

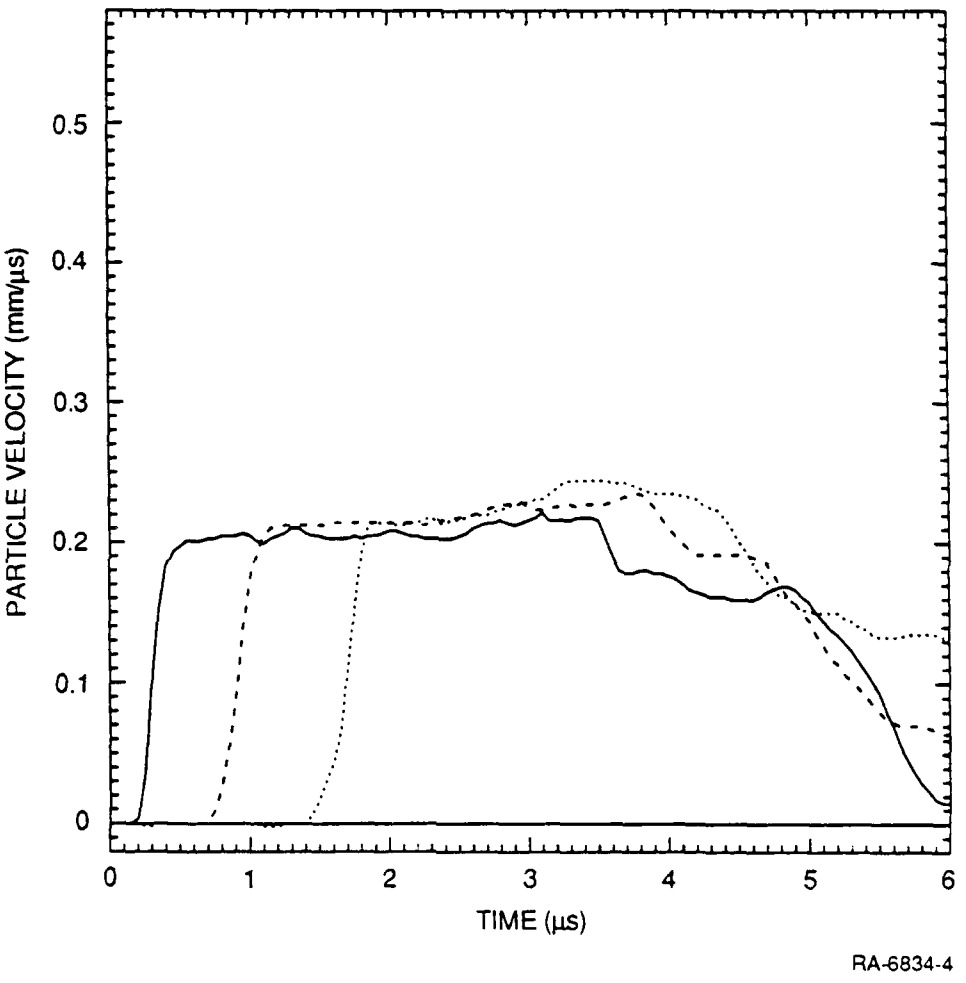

Figure 4-6. Composite plot of Lagrange longitudinal particle velocity histories in Composition B3 produced by parallel-inclined impact (15° angle) in Shot 85-2-9.

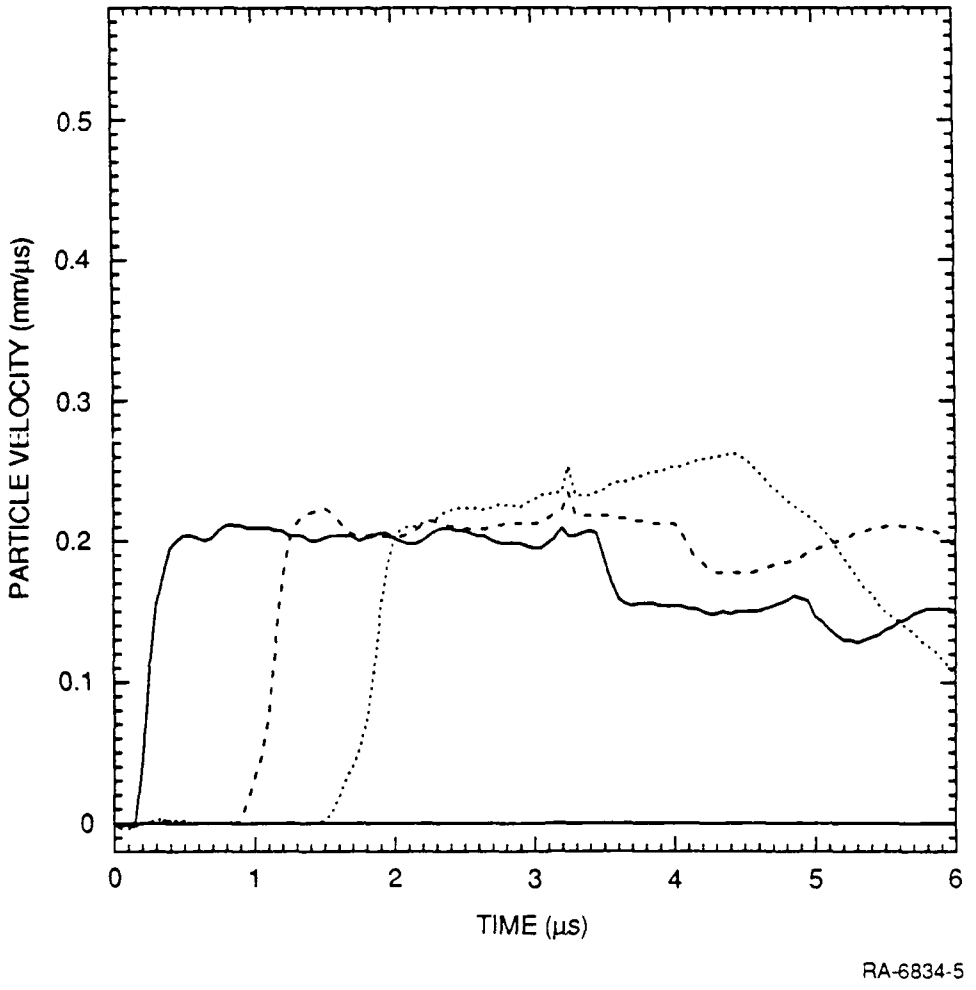

Figure 4-7. Composite plot of Lagrange longitudinal particle velocity histories in Composition B3 produced by parallel-inclined impact (20° angle) in Shot 85-2-10.

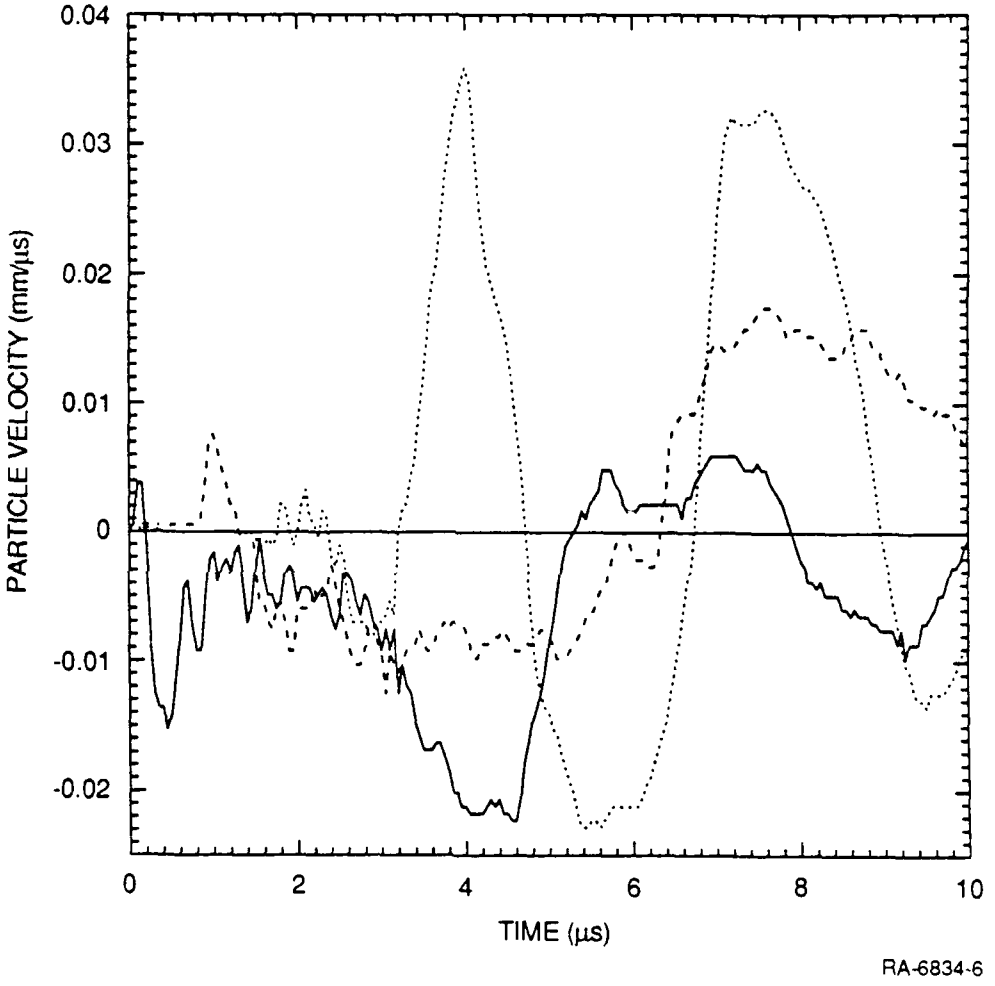

Figure 4-8. Records from shot 85-2-11, a parallel-inclined (15° angle) impact experiment designed to measure Lagrange shear particle velocity histories in Composition B3.

is that the energy release rate has a more pronounced on the flow produced in the normal impact experiment than on the flows produced in the PII experiments. The third is that all the sets of longitudinal particle velocity histories exhibit characteristics of type III flow influenced by CIR.

We conclude as a result of these observations that differences among the sets of longitudinal particle velocities recorded in Shots 85-2-8, 85-2-9, and 85-2-10 cannot be taken as evidence for the occurrence of SIR.

Because different conclusions were reached from the results of the second and third sets of experiments, and both sets of experiments were designed to produce initial compressional stresses in the 10-kbar region, we now asked why the sets of longitudinal particle velocity histories provide conflicting evidence for the occurrence of SIR. The only obvious answer is that the sets of longitudinal particle velocity histories recorded in the second and third sets of gas gun experiments exhibit different flow features because these sets of experiments were performed with different batches of Composition B3. This answer led us to suspect that the batches of Composition B3, seemingly cast under the same conditions, had different physical characteristics.

4.2.4 The Fourth Set of Shots

Because different results were obtained in the second and third sets of experiments, the fourth set was again designed to produce an initial compressional stress in Composition B3 in the 10-kbar region. The magnetic field was oriented to measure the longitudinal particle velocities produced by normal impact in Shot 86-2-16 and by PII (15° angle) in Shots 86-2-17 and 86-2-18. These experiments were again performed with a 3/8-inch-thick fused silica flyer. The velocity of the flyer was 0.294 mm/μs in Shot 86-2-16, 0.304 mm/μs in Shot 86-2-17, and 0.294 mm/μs in Shot 86-2-18. Figure 4-9 shows a composite plot of the longitudinal particle velocity histories recorded in Shot 86-2-17. The records from Shot 86-2-16 are not presented because they are excessively noisy, and those from Shot 86-2-18 are not presented because the second particle velocity gage was found to be inoperative in this experiment.

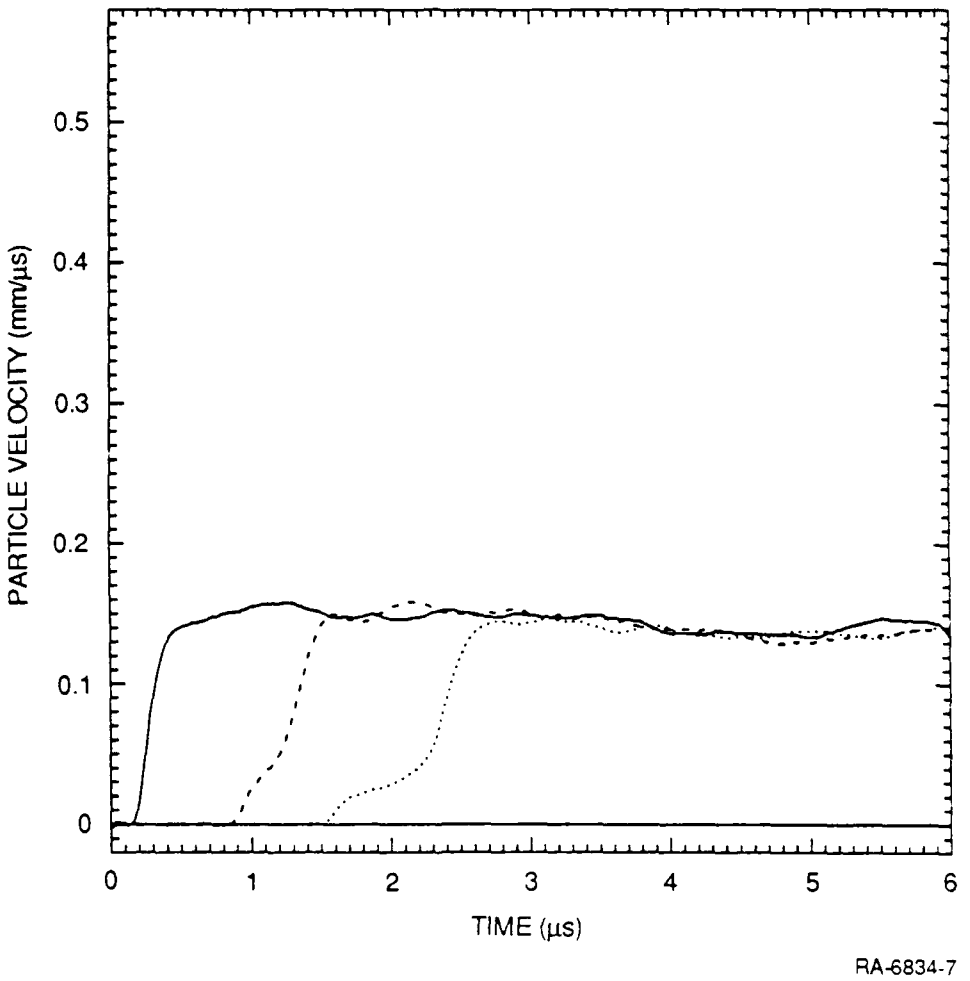

Figure 4-9. Composite plot of Lagrange longitudinal particle velocities in Composition B3 produced by parallel-inclined impact (15° angle) in Shot 86-2-17.

Examination of the composite plot in Figure 4-9 showed that a flow of type I exhibiting little evidence of CIR and no evidence of SIR is produced in Shot 86-2-17. Comparison of the particle velocity histories in Figure 4-9 with those in Figures 4-3(b) and 4-6, which were produced by similar flyer velocities, then showed that anomalously low particle velocities were recorded in Shot 86-2-17. This anomalous result and the observation from Figure 4-9 that the formation of a precursor wave is more evident in Shot 86-2-17 than in any of the other experiments were taken as further evidence that Composition B3 targets prepared in different castings had different physical properties.

4.2.5 The Fifth Set of Shots

Because anomalous particle velocities were recorded in the fourth set of experiments and flows of type III were produced in the first set of experiments, the fifth set of experiments was designed to produce initial compressional stresses in Composition B3 in the 10- and 15-kbar regions. The magnetic field was oriented to measure the longitudinal particle velocities produced by normal impact in Shots 86-2-64 and 86-2-67 and those produced by PII (15° angle) in Shots 86-2-65 and 86-2-66. A 3/8-inch-thick fused silica flyer was again used in all of these experiments. Composite plots of the longitudinal particle velocities recorded in Shot 86-2-64 (0° angle), with the flyer travelling at 0.293 mm/μs; in Shot 86-2-65 (15° angle), with the flyer travelling at 0.302 mm/μs; in Shot 86-2-66 (15° angle) with the flyer travelling at 0.452 mm/μs; and in Shot 86-2-67 (0° angle), with the flyer travelling at 0.429 mm/μs, are shown in Figures 4-10 through 4-13.

Superposition of the composite plots in Figures 4-10 and 4-11 shows that the particle velocity histories recorded in Shots 86-2-64 and 86-2-65 are essentially identical and show little evidence of exothermic reaction. Further examination of these sets of particle velocity histories again leads to two alternative interpretations of these flows; these interpretations have already been discussed (see Section 4.2.2) in our consideration of the particle velocity histories shown in Figures 4-3(a) and 4-3(b). Here for practical purposes we neglect the decaying step shock associated with a negative energy release rate and claim that

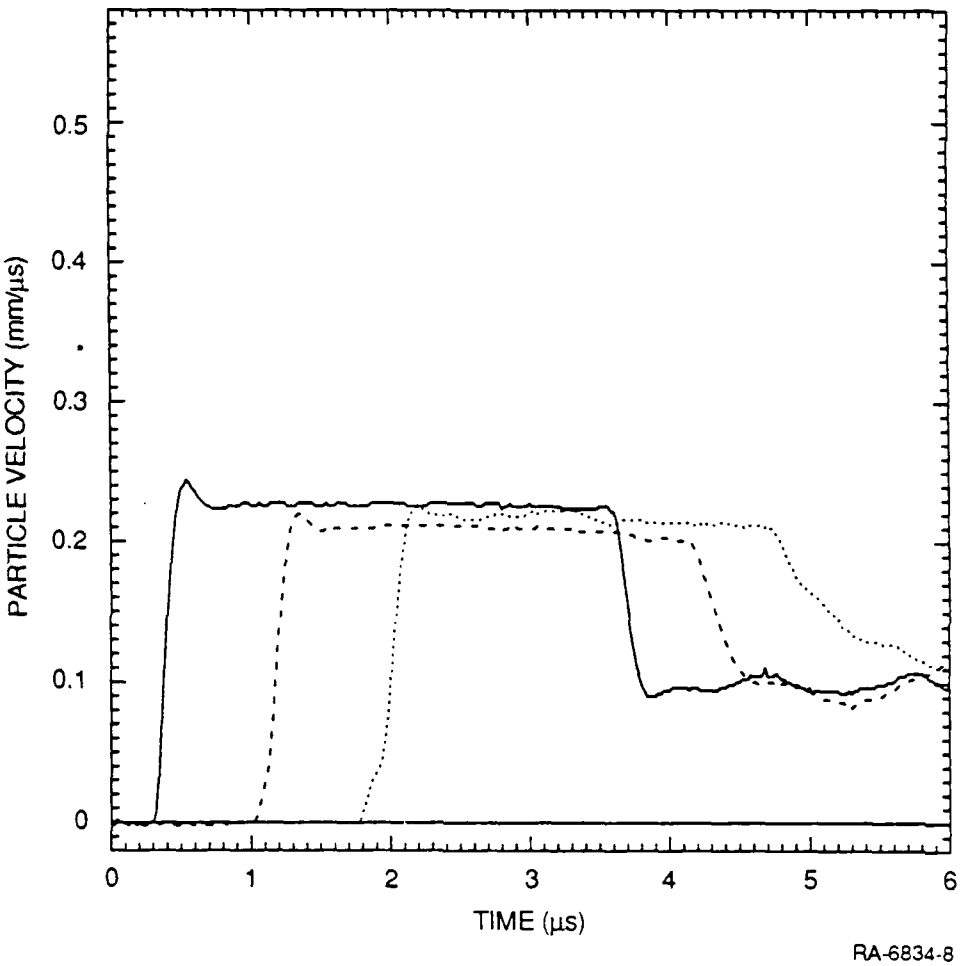

Figure 4-10. Composite plot of Lagrange longitudinal particle velocity histories in Composition B3 produced by normal impact in Shot 86-2-64.

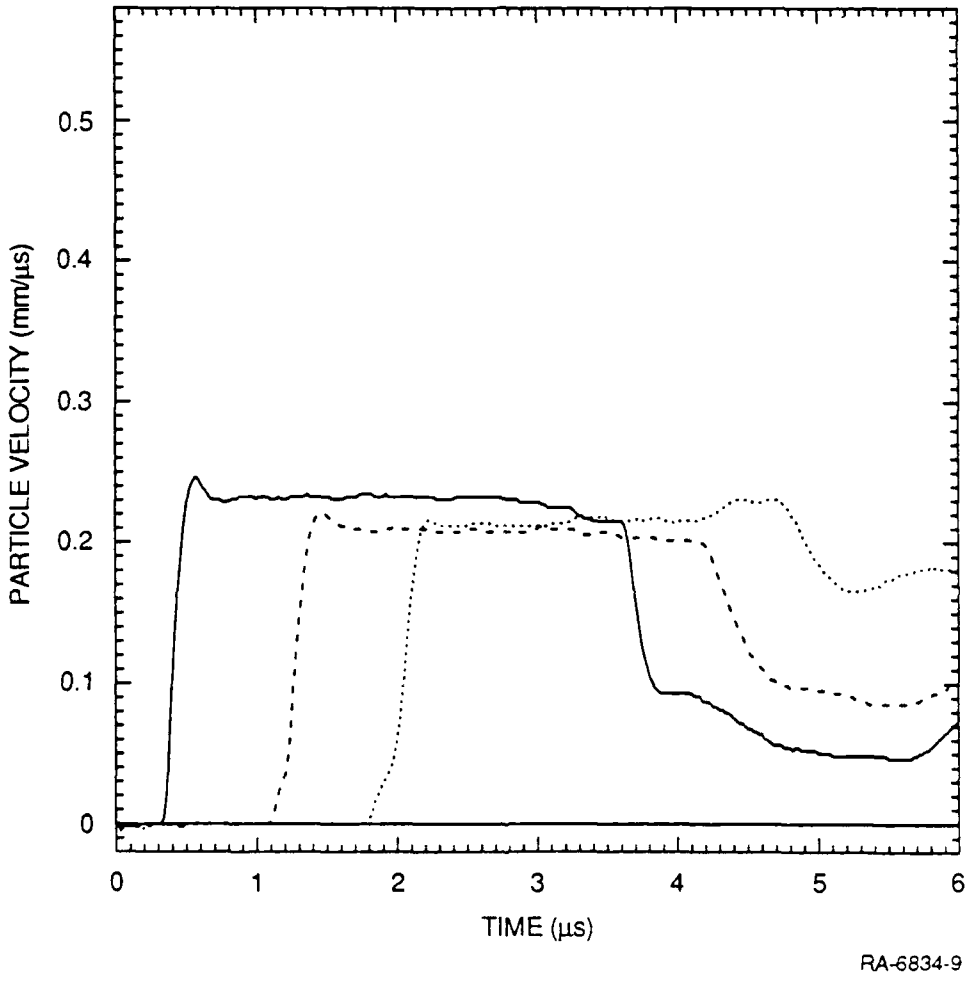

Figure 4-11. Composite plot of Lagrange longitudinal particle velocity histories in Composition B3 produced by parallel-inclined impact (15° angle) Shot 86-2-65.

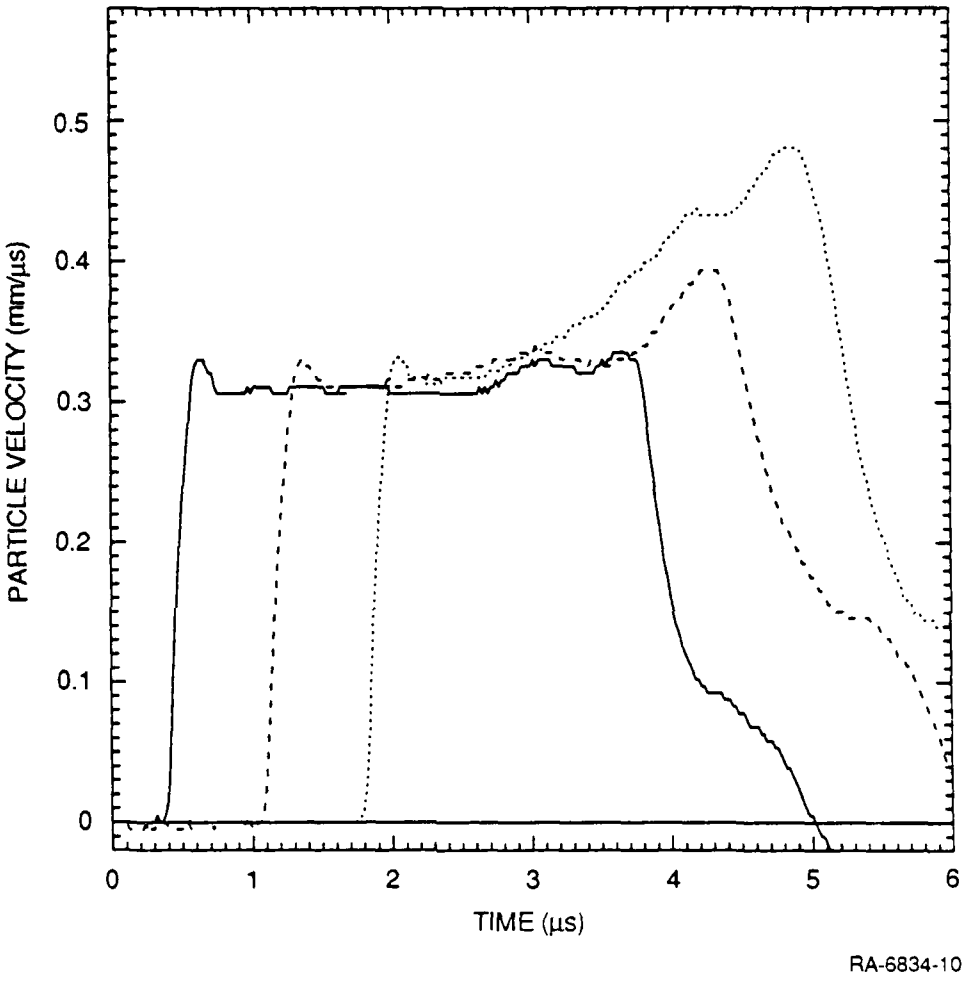

Figure 4-12. Composite plot of Lagrange longitudinal particle velocity histories in Composition B3 produced by parallel-inclined impact (15° angle) in Shot 86-2-66.

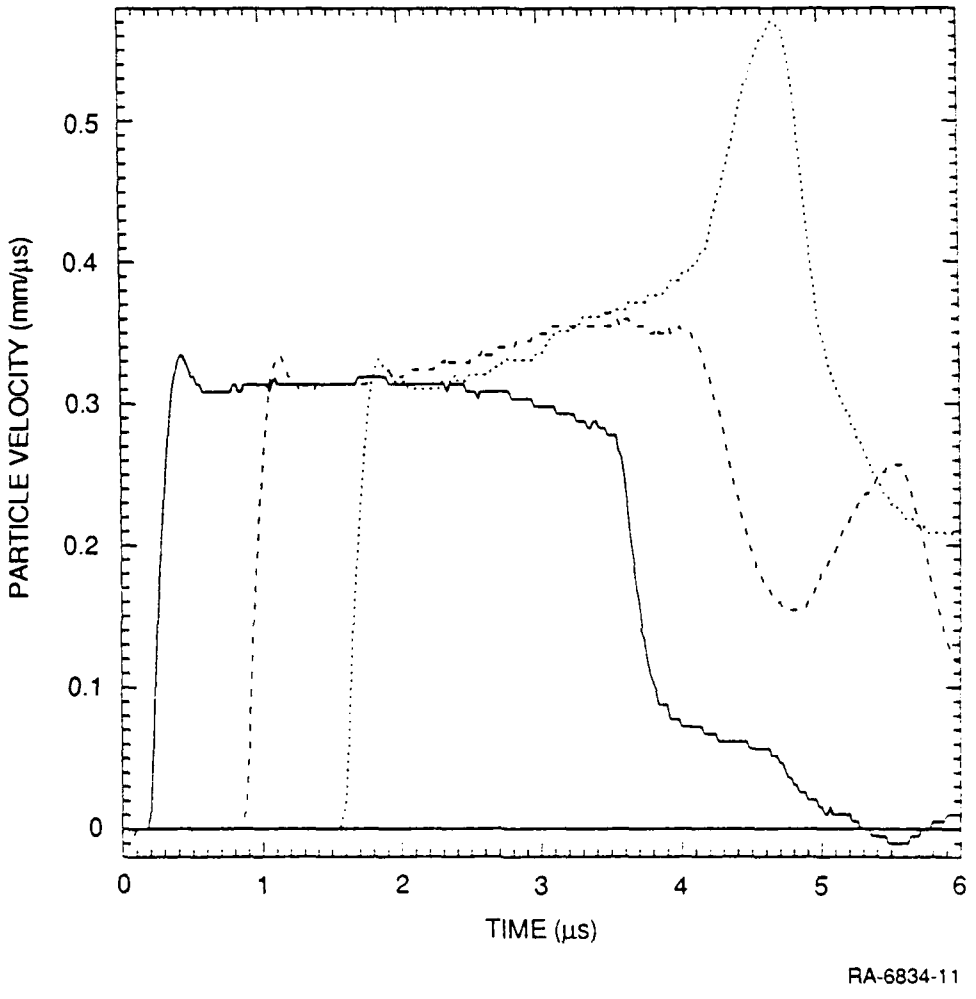

Figure 4-13. Composite plot of Lagrange longitudianl particle velocity histories in Composition B3 produced by normal impact in Shot 86-2-67.

the flows produced by normal-impact and PII in Shots 86-2-64 and 86-2-65 are nonreactive flows of type I.

Superposition of the composite plots in Figures 4-12 and 4-13 shows that the flows produced by normal-impact and PII in Shots 86-2-67 and 86-2-66 are initially identical (for about 2.3 μs), but then become markedly different. After 2.3 μs, the stress gradient at the first gage position becomes negative in Shot 86-2-66 but positive in Shot 86-2-67, and this difference between the flows produced by PII and normal impact cannot be neglected. Thereafter, the particle velocity histories recorded at the second and third gage positions in both experiments exhibit significant reactive flow features typical of a type III flow, but the reaction has a more pronounced influence in the flow produced by normal impact than in that produced by PII.

In the light of our theoretical discussions about reactive flows produced in gas gun experiments, we conclude that these differences between the sets of longitudinal particle velocity histories recorded in Shots 86-2-66 and 86-2-67 can be taken as evidence for SIR produced by PII.

5. CONCLUSIONS AND RECOMMENDATIONS

Experimental and theoretical studies of compression and shear wave propagation in Composition B3 were performed to establish the occurrence of shear-induced reaction (SIR) and provide a better understanding of its influence on the one-dimensional flow produced in an explosive by the type of parallel-inclined impact (PII) experiment pioneered by Gupta.[4]

Our theoretical study was based on a model analysis of the PII experiment with the shock-loaded target treated as an inert elastic solid and the resulting flow treated ideally as a pure compression wave followed by a pure shear wave. A complete equation of state (EOS) for a reactive elastic solid was formulated and used to derive the thermodynamic equations governing the one-dimensional adiabatic flows produced by PII. The conditions an elastic solid subjected to PII must satisfy to support our ideal inert flow were then formulated and used to construct the most convenient model EOS for investigating the reactive adiabatic flows produced in solids by normal-impacts and PIIs. Flows influenced by compression-induced reaction (CIR) and by SIR were then considered to show how the energy released by chemical reaction influences the longitudinal particle velocity field. The results of this consideration of reactive flow in a solid were then used to formulate a framework for interpreting the results of our gas gun experiments.

Our experimental study was based on Gupta's premise that significant differences between the sets of longitudinal particle velocity histories recorded in an explosive subjected to normal-impact and PII producing equivalent nonreactive compression waves can be taken as evidence for the occurrence of SIR in the PII experiment. Eighteen normal-impact and PII experiments were performed in a gas gun with Composition B3 targets, and multiple Lagrange gages embedded in these explosive targets were used to make longitudinal and shear particle velocity measurements. The eighteen experiments were divided into five sets that were performed with targets

made from different batches of Composition B3. The results of the longitudinal particle velocity measurements gave evidence for the occurrence of SIR in the first batch of Composition B3, which was shocked initially into the 10-kbar region, and in the fifth batch of Composition B3, which was shocked initially into the 15-kbar region. The results of the shear particle measurements led to the conclusion that the shear deformation produced in Composition B3 by PII remains close to the impact surface.

We took a simplistic approach to the propagation of compression and shear waves in explosives by treating the explosive as an elastic solid governed by an equation-of-state that decouples the longitudinal and shear deformations when the flow is nonreactive. This approach is relevant in the light of our experimental approach to SIR because it allows us to concentrate on reactive flow and the influence of chemical reaction on the longitudinal particle velocity field. It is clear that such an understanding of reactive flow is required to interpret the sets of longitudinal particle velocity histories recorded in equivalent normal-impact and PII experiments and attribute significant differences in their reactive flow features to SIR.

The results of our theoretical study substantiate and provide a more detailed, qualitative account of Gupta's experimental approach to SIR, but they also show that the complex nature of reactive flow makes this approach more complicated than was originally thought. A more quantitative procedure is needed for interpreting the sets of longitudinal particle velocity histories recorded in the gas gun experiments. Additional work is also required to understand why no well-defined shear particle velocity histories were recorded in our PII experiments with Composition B3.

Although the results of our gas gun experiments with Composition B3 provide evidence for the occurrence of SIR produced by PII, they are inconsistent and therefore not totally convincing. Because experimental conditions were essentially the same in the second, third, and fourth sets of experiments, inconsistencies among the sets of longitudinal particle velocity histories recorded in these experiments must be

attributed to differences among the Composition B3 targets. It thus follows that our casting procedure produced batches of Composition B3 targets with different physical properties and was not as well controlled as we had originally thought. More attention must be given to the casting procedures used to make targets for the gas gun experiments.

We conclude that the results of our theoretical and experimental studies provide evidence for the occurrence of SIR in explosives subject to PII, but not enough to establish that SIR plays a significant role in the shock initiation of explosives. We recommend that any future theoretical study of SIR be based on a more realistic description of an explosive. This description can then be used to develop a more quantitative procedure for interpreting the sets of longitudinal particle velocity histories recorded in equivalent normal-impact and PII experiments and also to determine why no well-defined shear particle velocity histories were recorded in our PII experiments. We finally recommend that any future gas gun investigations of SIR be performed with explosive targets with similar physical properties produced by a well-proved casting technique.

REFERENCES

1. In 1940, P. W. Bridgman studied the response of explosives under superposed shear and pressure; these studies were reported in J. Chem. Phys. 15, 311 (1947). In 1960, in the introduction to his Collected Experimental Papers, Vol. I (Harvard University Press, 1964), Bridgman noted the difficulty of detecting a true chemical instability under the combination of compression and shear. He recommended the need for further experimental efforts to confirm his conjectures in the 1940s.

2. C. S. Coffey, M. J. Frankel, T. P. Liddiard, S. J. Jacobs, "Experimental Investigation of Hot Spots Produced by High Rate Deformation and Shocks," in Seventh Symposium (International) on Detonation (NSWC MP82-334, 1982), pp. 970-975.

3. Y. M. Gupta, Presentation at the DOD Workshop "New Opportunities for Research in Energetic Materials," Wrightsville Beach, North Carolina (November 1977).

4. Y. M. Gupta, Appl. Phys. Lett. 29, 694 (1976).

5. Y. M. Gupta, D. D. Keough, D. F. Walter, K. C. Dao, D. Henley, A. Urweider, Rev. Sci. Instr. 51, 183 (1980).

6. Y. M. Gupta, "Development of a Method for Determining Dynamic Shear Properties," Final Technical Report to DNA Headquarters, Washington D.C., under Contract No. DNA 001-76-C-0384, SRI International, Menlo Park CA 94025 (May 1978); also see Polym. Eng. Sci. 24, 851 (1984).

7. R. N. Thurston, "Waves in Solids," in Encyclopedia of Physics, Vol. VIa/4, Mechanics of Solids IV (Springer-Verlag, Berlin, Heidelberg, New York, 1974), pp. 109-146.

8. H. Flanders, Differential Forms (Academic Press, New York, London, 1963).

9. C. Truesdell and R. Toupin, "The Classical Field Theories," in Encyclopedia of Physics, Vol. III/1, Principles of Classical Mechanics and Field Theory (Springer-Verlag, Berlin, Gottingen, Heidelberg, 1960), p. 246.

10. J. W. Gibbs, The Scientific Papers of J. Willard Gibbs, Vol. 1, Thermodynamics (Dover Publications, Inc., New York, 1961), pp. 184-214.

11. G. R. Fowles and R. F. Williams, J. Appl. Phys. 41, 360 (1971).

12. M. Cowperthwaite and R. F. Williams, J. Appl. Phys. 42, 456 (1971).

13. R. Courant and K. O. Friedrichs, Supersonic Flow and Shock Waves (Interscience Publishers, Inc., New York, 1948), p. 94.

14. W. Fickett and W. C. Davis, Detonation (University of California Press, Berkeley, Los Angeles, London, 1979), p. 4.

15. M. Cowperthwaite and J. T. Rosenberg, "A Multiple Lagrange Gage Study of the Shock Initiation Process in Cast TNT," Sixth Symposium (International) on Detonation (ACR-221, Office of Naval Research, 1976), pp. 786-793.

16. R. Weingart, R. Barlett, S. Cochman, L. Erickson, J. Chan, J. Janzen, R. Lee, D. Logan, and J. T. Rosenberg, "Manganin Stress Gages in Reacting High Explosive Environment," Symposium H.D.P., Behavior of Dense Media Under High Dynamic Pressures (Editions du Commissariat á l'Energie Atomique, Centre d' Etudes Nucléaires de Saclay, 1978), pp. 451-461.